

Aberystwyth University

Age determination using feldspar:

King, Georgina ; Burow, Christoph; Roberts, Helen M.; Pearce, Nicholas

Published in:

Radiation Measurements

DOI:

[10.1016/j.radmeas.2018.07.013](https://doi.org/10.1016/j.radmeas.2018.07.013)

Publication date:

2018

Citation for published version (APA):

King, G., Burow, C., Roberts, H. M., & Pearce, N. (2018). Age determination using feldspar: Evaluating fading-correction model performance. *Radiation Measurements*, 119, 58-73.
<https://doi.org/10.1016/j.radmeas.2018.07.013>

General rights

Copyright and moral rights for the publications made accessible in the Aberystwyth Research Portal (the Institutional Repository) are retained by the authors and/or other copyright owners and it is a condition of accessing publications that users recognise and abide by the legal requirements associated with these rights.

- Users may download and print one copy of any publication from the Aberystwyth Research Portal for the purpose of private study or research.
- You may not further distribute the material or use it for any profit-making activity or commercial gain
- You may freely distribute the URL identifying the publication in the Aberystwyth Research Portal

Take down policy

If you believe that this document breaches copyright please contact us providing details, and we will remove access to the work immediately and investigate your claim.

tel: +44 1970 62 2400
email: is@aber.ac.uk

Accepted Manuscript

Age determination using feldspar: Evaluating fading-correction model performance

Georgina E. King, Christoph Burow, Helen M. Roberts, Nicholas J.G. Pearce

PII: S1350-4487(17)30477-8

DOI: [10.1016/j.radmeas.2018.07.013](https://doi.org/10.1016/j.radmeas.2018.07.013)

Reference: RM 5962

To appear in: *Radiation Measurements*

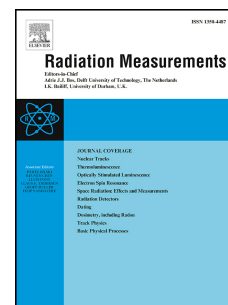
Received Date: 12 July 2017

Revised Date: 31 May 2018

Accepted Date: 16 July 2018

Please cite this article as: King, G.E., Burow, C., Roberts, H.M., Pearce, N.J.G., Age determination using feldspar: Evaluating fading-correction model performance, *Radiation Measurements* (2018), doi: 10.1016/j.radmeas.2018.07.013.

This is a PDF file of an unedited manuscript that has been accepted for publication. As a service to our customers we are providing this early version of the manuscript. The manuscript will undergo copyediting, typesetting, and review of the resulting proof before it is published in its final form. Please note that during the production process errors may be discovered which could affect the content, and all legal disclaimers that apply to the journal pertain.



Age determination using feldspar: evaluating fading-correction model performance

Georgina E. King^{*,1,2}, Christoph Burow³, Helen M. Roberts² and Nicholas J.G. Pearce²

¹Institute of Geological Sciences and Oeschger Centre for Climate Change Research, University of
Bern

²Department of Geography and Earth Sciences, Aberystwyth University

³Institute of Geography, University of Cologne

*georgina.king@gmail.com

Abstract

The recent introduction of post-IR IRSL measurement protocols has prompted a resurgence in luminescence applications using feldspar, some of which are affected by anomalous fading related signal loss. Many fading-corrected feldspar ages are reported in the literature, however few of those ages have been corrected using the model of Huntley (2006) [Huntley, D.J., 2006. *An explanation of the power-law decay of luminescence. Journal of Physics: Condensed Matter* 18(4), 1359-1365]. Here we present a new **R** function that calculates fading-corrected ages using the model of Huntley (2006), implemented with either a single-saturating exponential (1EXP) or general-order kinetic (GOK) fit. We evaluate the performance of the model through (i) contrasting measured and modelled field saturation values for a suite of 41 published saturated samples, and (ii) through using the model to fading-correct feldspar ages of samples with independent age control. Our results indicate that when implemented with 1EXP this model has an accuracy of 10 % for predicting sample saturation, but that independent ages may be overestimated when the model is used to fading-correct samples across a range of timescales. In contrast, providing that the dose response curve has been characterised beyond 600 Gy, implementing the Huntley (2006) model with a GOK fit yields accurate age estimations. Modelled age overestimation for 1EXP is associated with dose response curve deviation from a single saturating exponential. Finally we contrast the laboratory measured light levels of a suite of 50 saturated samples with their corresponding fading rates. We show that these saturated samples may yield D_e values below $2D_0$, and thus that $2D_0$ is not an effective screening criterion for sample saturation where no anomalous fading correction is made.

1. Introduction

Since the introduction of post-infrared infrared stimulated luminescence (post-IR IRSL) measurement protocols (Thomsen et al., 2008; Buylaert et al., 2009; Li and Li, 2011; Thiel et al., 2011), which measure signals that are less affected by anomalous fading (i.e. athermal signal loss over time due to quantum mechanical tunnelling), there has been a rapid uptake of these new methods in the luminescence dating community. However, high temperature post-IR IRSL signals are hard to bleach in nature (e.g. Kars et al., 2014; Zhang et al., 2015), resulting in the proposal of lower temperature post-IR IRSL measurements for young (e.g. Reimann and Tsukamoto, 2012) or poorly bleached sediments (e.g. Kars et al., 2014). Whilst not suffering from anomalous fading to the same extent as the IRSL₅₀ feldspar signal, low-temperature post-IR IRSL signals often require fading-correction, arguably limiting the benefits of post-IR IRSL measurement protocols. On the basis that fading measurements of quartz minerals (a mineral thought not to fade) yield g_{2days} values of up to 0.98 ± 0.09 %/decade, Buylaert et al. (2012) suggested that it may not be appropriate to fading correct post-IR IRSL signals which yield g_{2days} values of 1-1.5 %/decade. However, non-negligible fading rates (i.e. >1.5%/decade) have been reported for post-IR IRSL₂₂₅ and even for post-IR IRSL₂₉₀ measurements (e.g. Lowick et al., 2012; Lauer et al., 2017), indicating a requirement for fading-correction. Finally, the development of low-temperature OSL-thermochronometry, which utilises low temperature IRSL signals, requires accurate fading-correction in order to model luminescence signal accumulation under changing thermal conditions (e.g. Guralnik et al., 2015a; King et al., 2016a; Valla et al., 2016).

Various models for anomalous fading have been proposed, which can be used to correct luminescence ages (e.g. Aitken, 1985; Lamothe and Auclair, 1999; 2000; Huntley and Lamothe, 2001; Lamothe et al., 2003; Huntley, 2006). The model of Huntley and Lamothe (2001) is the most widely used approach but is only applicable to the linear part of the dose response curve, although experiments by Buylaert et al. (2008) indicate that it may also be effective beyond this range. A function for age correction using the Huntley and Lamothe (2001; H+L) approach has been implemented in the **R** package 'Luminescence' (Kreutzer et al., 2012; 2018) and is commonly used to correct feldspar luminescence ages (e.g. Bickel et al., 2015; Diaz et al., 2016). The dose rate correction method (DRC) of Lamothe et al. (2003) has the advantage of potentially being applicable over the full range of the dose response curve, and has also been successfully applied in some studies (Auclair et al., 2007; Buylaert et al., 2009; Kars and Wallinga, 2009). Huntley (2006) proposed a model on the premise that rates of fading can be explained by the density and distance of recombination centres from the IRSL trap. Kars et al. (2008) and Li and Li (2008) used this model together with a single-saturating exponential fit (1EXP) to evaluate measured luminescence data, and Kars and Wallinga (2009) also

investigated the impact of charge trapping competition on rates of athermal loss. Guralnik et al. (2015a) also used the Huntley (2006) model to fading correct bedrock thermochronometry samples, but implemented it with a general-order kinetic (GOK) fit. Here we evaluate the Huntley (2006) model for age fading correction, using a new **R** function that is freely available in the ‘Luminescence’ package (v.0.8.1, Kreutzer et al., 2012; 2018), `calc_Huntley2006()`, (King and Burow, 2018) which calculates fading-corrected ages and sample specific field saturation values, from which the ability to derive a finite age can be evaluated. We highlight the effects of fading over laboratory timescales and show why $2D_0$ is not an effective screening criterion for sample saturation for samples which experience anomalous fading.

2. The model

Huntley (2006) proposed a model that explains the power-law decay of luminescence signals through tunnelling. Various detailed descriptions of this model have been given in the literature (cf. Kars et al., 2008; Kars and Wallinga, 2009; Li and Li, 2008; Morthekai et al., 2011; King et al., 2016a) and it is only briefly described here. The model is based on the premise that a trapped electron will tunnel to its nearest neighbouring recombination centre, with the lifetime of trap occupancy governed both by recombination centre density (ρ) and recombination centre distance from the electron trap (r), (Figure 1). The density of recombination centres is assumed to be much greater than trapping centres (Huntley, 2006) and can be quantified from fading measurements (for example using the `analyse_FadingMeasurement()` function in the **R** package ‘Luminescence’, Kreutzer and Burow (2017)), whereby the luminescence signal remaining after increasing measurement delays is fitted with equation 5 of Kars et al. (2008):

$$IRSL_{faded} = IRSL_{initial} e^{-\rho' \ln(1.8 s t^*)^3} \quad [1]$$

where $IRSL_{faded}$ is the luminescence signal measured at time t^* , which is the time between irradiation and measurement, including half the time of irradiation (after Auclair et al., 2003). $IRSL_{initial}$ is the luminescence signal without any anomalous fading, ρ' is the dimensionless density of recombination centres and s is $3 \times 10^{15} \text{ s}^{-1}$ following Huntley (2006), which is the attempt-to-escape frequency of an electron from an atom-sized box.

[Figure 1]

Li and Li (2008), Kars et al. (2008), Kars and Wallinga (2009) and Valla et al. (2016) have investigated the model of Huntley (2006) in detail, and we review their investigations here. The Huntley (2006) model is based on the assumption that the density of recombination centres, ρ , remains effectively constant. However, following Huntley and Lian (2006), Li and Li (2008) proposed that a changing density of recombination centres may be required to account

for laboratory measured fading-rate dose-dependency which has been reported in a number of studies (Huntley and Lian, 2006; Kars et al., 2008; Li and Li 2008). Li and Li (2008) observed that for sample Sm1, the g-values (normalised to $t_c = 1200$ s, rather than 2 days) increased from 3.1 ± 0.3 %/decade to 5.4 ± 0.2 %/decade with given doses of 32 and 2050 Gy respectively (Figure 2A). However where they plotted the normalised natural luminescence signals (L_{nat}) of the same sample suite against their estimated palaeodoses, the data can be well described by a single saturating exponential dose response curve predicted from a single density of recombination centres using the Huntley (2006) model (Figure 2B). It is unclear how this discrepancy can be reconciled. Kars and Wallinga (2009) tested the performance of the Huntley (2006) model, as implemented for age fading correction by Kars et al. (2008) for a suite of samples with independent age control. Using a single saturating exponential curve for dose response, Kars and Wallinga (2009) obtained fading-corrected ages commensurate with, albeit older than independent ages. Following Huntley and Lian (2006) and Wallinga et al. (2007), Kars and Wallinga (2009) also investigated whether charge-trapping competition effects with increasing dose could affect model performance. However, they found that incorporation of charge trapping competition led to greater deviation between fading corrected ages and independent age controls. Valla et al. (2016) evaluated the performance of the Huntley (2006) model as implemented by Guralnik et al. (2015a), i.e. using a general order kinetic model (Guralnik et al., 2015b) rather than a single saturating exponential fit for dose response. Valla et al. (2016) contrasted laboratory measured saturation ratios with those predicted for athermal steady state for 32 bedrock samples, recording a correlation between measured and modelled levels of saturation for some samples, inferring that the majority of their dataset reflected athermal signal loss rather than rock cooling histories. Our study complements the earlier work of Kars et al. (2008), Li and Li (2008), Kars and Wallinga (2009) and Valla et al. (2016) through evaluating how well the Huntley (2006) model can predict field saturation for 41 saturated samples taken from existing literature when implemented with 1EXP or GOK, and also its age fading correction performance for a further suite of samples with independent age controls.

[Figure 2]

3. The function

The `calc_Huntley2006()` function, which has been recently added to the **R** package 'Luminescence', requires the user to input:

- the regenerative dose times used to measure the dose response curve (s),
- the sensitivity corrected luminescence data (i.e. L_x/T_x , a.u.) and their individual uncertainties,

- the reader dose rate \dot{D}_{reader} (Gy s⁻¹) on which the Lx/Tx data were measured,
- the environmental dose rate \dot{D} (Gy ka⁻¹), and
- the sample specific ρ' (dimensionless).

Calculation of the model comprises three stages:

(1) Simulation of an unfaded dose response curve for the given \dot{D}_{reader} and ρ' , from which the sample's level of saturation (n/N) can be calculated (e.g. Figure 3), where n is the number of trapped electrons and N is the maximum number of electron traps.

(2) Simulation of a natural dose response curve for the given \dot{D} , ρ' and unfaded D_0 (e.g. Figure 3) from which the fading-corrected age can be determined through interpolation of the sensitivity corrected natural signal, L_{nat} .

(3) Determination of field steady-state (i.e. the equilibrium between charge trapping due to exposure to ionizing radiation and charge detrapping due to athermal loss), $(n/N)_{ss}$, for the given \dot{D} , ρ' and unfaded D_0 .

The simulated unfaded and natural dose response curves, as well as the laboratory measured dose response curve are shown in the `calc_Huntley2006()` model output (Figure 3), enabling comparison of the different levels of saturation and the influence of anomalous fading on laboratory, and natural dose response.

[Figure 3]

4. Model performance

4.1 Determining natural signal saturation

In order to test the performance of the model of Huntley (2006), we have contrasted the measured (n/N) values of a range of different saturated samples reported in the literature, with their calculated (n/N)_{ss} values calculated either using 1EXP or GOK (Figure 4). Kars et al. (2008) tested the performance of this model implemented with 1EXP for five saturated samples from the Lower Rhine (reported average value included in Figure 4), and observed that the model underestimated the average measured field saturation level by 9 % (note that no information on scatter between the five samples is given in the original publication). We have also calculated (n/N)_{ss} for the IRSL₅₀ and post-IR IRSL₂₉₀ signals of sample 62213 (for both early and late background subtraction) reported in Thomsen et al. (2011), and also report data for a number of saturated bedrock samples, which were measured as the limitations of OSL-thermochronometry were explored (Guralnik et al., 2015a; Valla et al., 2016; King et al., 2016b).

Only samples with adequate independent age control, confirming their saturation, have been included; the data used to produce Figure 4 are summarised in Table 1. Where a 1EXP fit is used, the majority of the samples investigated here, which are derived from a variety of different geological and geographical settings, exhibit (n/N) within 10 % of $(n/N)_{ss}$ (Figure 4A). In contrast where a GOK fit is used, the data are more scattered and exhibit a trend towards overestimation of $(n/N)_{ss}$ relative to (n/N) (Figure 4B). The cause of the discrepancy between these two model implementations is unclear, but may indicate that feldspar do not follow GOK dose response in the natural environment (cf. Li and Li, 2012), which is discussed further below. The data in Figure 4A indicate that the Huntley (2006) model has approximately 10 % accuracy when applied with a 1EXP fit, but that there is no apparent systematic bias towards over or underestimation of sample field saturation. The scatter in the 1EXP results likely reflects uncertainties in the laboratory-constrained rates of anomalous fading and dose response. Huntley and Lian (2006) report differences in rates of anomalous fading between individual aliquots of the same sample, by up to a factor of two, and some of this scatter may also be related to averaging of anomalous fading rates.

[Figure 4]

4.2 Fading-correction: Comparison with independent age control

The adequacy of any fading model is determined by its ability to accurately correct ages. Kars and Wallinga (2009) investigated the performance of the Kars et al. (2008) implementation of the Huntley (2006) model with 1EXP on a suite of samples from Bortel, for which quartz OSL ages from 15 ka to 325 ka provided age control. Although contrasting luminescence chronologies can be limited by commonalities in \dot{D} and D_e values, such comparisons are often practical. Kars and Wallinga (2009) report that whereas one feldspar age overestimated its partner quartz age by 150 ka (175 %), the remaining 10 samples exhibited better agreement, whilst all systematically overestimating the quartz ages. Incorporating charge trapping competition effects into the model resulted in greater discrepancies between quartz and feldspar fading-corrected ages (Kars and Wallinga, 2009, their Figure 1) and is not considered here. Morthekai et al. (2011) also investigated applying the approach of Kars et al. (2008) and Huntley and Lamothe (2001) to fading-correct basaltic feldspars with known ages ≥ 400 ka. They found that both methods underestimated sample age, and furthermore that the approach of Huntley and Lamothe (2001) exhibited more severe (~ 80 %) age underestimations. More recently Li et al. (2018) used the Kars et al. (2008) and Lamothe et al. (2003) approaches to fading correct ages of samples from the Heidelberg Basin, Germany. From contrasting their resulting ages with a palaeomagnetic stratigraphy, they determined that the

Kars et al. (2008) model gave more reliable results. In this study, we evaluate performance of the Huntley (2006) model for the IRSL₅₀ signals of two sets of sedimentary samples with independent age control. The first sample set (GOS/ZEL) are from Lowick et al. (2012) and the second set (MFRB/BRR) are from this study.

4.2.1 Sample details

GOS3 and GOS4

Polymineral fine-grained samples GOS3 and GOS4 were taken from the Gossau gravel pit in Kanton Zürich, Switzerland (Preusser, 1999; 2003), which hosts some of the most comprehensively investigated Marine Isotope Stage 3 sediments in this region (the Gossau-Interstadial-Complex). The samples were collected from overbank deposits adjacent to previously dated peat horizons (Figure 5). For sample GOS4 the adjacent peat has been dated to ~32.3 cal. ka BP using radiocarbon dating and 34.7 ± 4.0 ka using $^{230}\text{Th}/\text{U}$ TIMS (Geyh and Schlüchter, 1998; Preusser, 2003). Sample GOS3 is stratigraphically older, and overlies a peat horizon with radiocarbon ages of ~48.0-50.5 cal. ka BP (Schlüchter et al., 1987; Preusser, 2003) as well as a $^{230}\text{Th}/\text{U}$ TIMS age of 49.4 ± 3.3 ka (Geyh and Schlüchter, 1998). These samples have previously been dated using a multiple-aliquot IRSL approach, resulting in polymineral fine-grain ages of 51.8 ± 5.4 ka for GOS3 (Preusser, 1999) and 29.0 ± 3.9 ka for GOS4 (Preusser, 2003). More recently Lowick et al. (2012) used a 225 °C and 290 °C post-IR IRSL protocol to re-investigate these samples, resulting in fading-corrected ages of 60 ± 4 ka to 78 ± 10 ka for GOS3 and 41 ± 2 ka to 45 ± 4 ka for GOS4 dependent on signal and including IRSL₅₀ signals measured within the post-IR IRSL₂₂₅ protocol. Lowick et al. (2012) measured fading rates for two aliquots of a range of samples from Switzerland, including GOS3 and ZEL7 (see below). They found that measured $g_{2\text{days}}$ values were similar across the entire sample suite, resulting in average values of 2.33 ± 0.84 %/decade for the IRSL₅₀ signal measured within the post-IR IRSL₂₂₅ protocol, 1.62 ± 0.40 %/decade for the post-IR IRSL₂₂₅ signal and 2.13 ± 1.39 %/decade for the post-IR IRSL₂₉₀ signal. Lowick et al. (2012) used the approach of Huntley and Lamothe (2001) and these average $g_{2\text{days}}$ values for fading correction. Here we use the data of Lowick et al. (2012) for the IRSL₅₀ signal measured in the post-IR IRSL₂₂₅ protocol, in order to test fading-correction using the Huntley (2006) model. Rather than using the average $g_{2\text{days}}$ value, we use a $g_{2\text{days}}$ value of 2.65 ± 0.42 %/decade, determined for the IRSL₅₀ signal of sample GOS3 (Lowick et al., 2012 their Figure 2). As no value for sample GOS4 is reported in Lowick et al. (2012), we also use the value for GOS3 for this sample.

ZEL4 and ZEL7

Polymineral fine-grained samples ZEL4 and ZEL7 were collected from the 'Marti' gravel pit in the Luthern Valley of central Switzerland (Preusser et al., 2001). The samples are taken from a succession of fine-grained fluvial deposits (Figure 5), which are bracketed between two coarse-gravel units. A peat layer within these strata has been dated to 95 ± 3 ka using $^{230}\text{Th}/\text{U}$ TIMS (Geyh et al., 1997) and previous IRSL dating of these samples yielded a mean age of 96 ± 4 ka (Preusser et al., 2001; Lowick et al., 2012). Lowick et al. (2012) reported ages for samples ZEL4 and ZEL7 of between 107 ± 9 ka and 292 ± 36 ka following fading-correction of IRSL_{50} (measured in a post-IR IRSL_{225} protocol), post-IR IRSL_{225} and post-IR IRSL_{290} ages (using the average $g_{2\text{days}}$ values described above). Here we also use the data of Lowick et al. (2012) for the IRSL_{50} signal in order to test fading-correction using the Huntley (2006) model. A $g_{2\text{days}}$ value of 2.03 ± 0.93 %/decade was determined for this signal for sample ZEL7 (Lowick et al., 2012 their Figure 2). As no value for sample ZEL4 is reported in Lowick et al. (2012) we also use the value for ZEL7 for this sample.

BRR-2

Sample 205/BRR-2 was collected from Blackman Ridge Road ($46^{\circ}27'29''$ N, $118^{\circ}50'46''$ W), which comprises a 3.5 m exposure of the Palouse loess, Washington State, USA. The Mazama tephra (modern Crater Lake, Oregon, USA) has been identified at this site previously (Sweeney, pers. comm.), which is the most widespread Quaternary tephra on the Columbia Plateau (Busacca et al., 1992), and has been dated to 7.6 ± 0.2 ka BP (ice-core derived calendrical age from Zdanowicz et al., 1999). At this exposure, the Mazama tephra is diffuse and has been highly diluted by large volumes of loessic material which make it barely visible in the roadside exposure. Whilst diffuse the deposit is continuous and is interpreted as being in-situ. Sample 205/BRR-2 (0.85 m) underlies this diffuse tephra horizon by approximately 0.3 m (Figure 5). In addition, a sample of the tephra horizon (BRRMAZ) was also collected for major, minor and trace element chemical characterisation to confirm its assignment to the Mazama tephra.

MFRB-1 and MFRB-2

Samples 204/MFRB-1 and 204/MFRB-2 were taken from the McFeeley Road site ($46^{\circ}18'54''$ N, $118^{\circ}27'10''$ W) of the Palouse loess deposits of Washington State, USA. The section comprises a 3 m exposure containing a 30 cm thick tephra horizon which has been assigned to Glacier Peak using single-shard major-element analysis (Spencer and Knapp, 2010) and trace-element analyses (Kuehn et al., 2009). This tephra horizon has an age of 13.5 ± 0.1 cal. ka BP (Kuehn et al., 2009); sample 204/MFRB-2 (0.55 m) was taken 0.10 m above the tephra horizon, and sample 204/MFRB-1 (0.92 m) was taken 0.10 m below the tephra horizon (Figure

5). A sample of the tephra horizon (MFRGP) was also taken for minor, major and trace element chemical characterisation.

[Figure 5]

4.2.2 Tephra sample preparation, measurement & results

The tephra samples from BRR and MFRB were prepared using standard methods (cf. King et al., 2016c) in the Department of Geography and Earth Sciences at Aberystwyth University. Samples were wet sieved to obtain the 180-212 μm grain size, before density separation at 2.5 g cm^{-3} using sodium polytungstate to isolate the glass fraction from contaminating minerals. The extracted shards were mounted in resin and polished using increasingly fine polishing papers and suspensions ($\sim 25 \text{ }\mu\text{m}$ to $0.3 \text{ }\mu\text{m}$) and were finished using $0.02 \text{ }\mu\text{m}$ colloidal silica.

The major element chemistry of individual glass shards was measured using wavelength-dispersive electron probe microanalysis (EPMA) at the Research Laboratory of Archaeology and Art History at Oxford University. A JEOL 8600 electron microprobe with four wavelength-dispersive spectrometers was used to analyse ten major elements (Na, Mg, Al, Si, P, K, Ca, Ti, Mn and Fe). An accelerating voltage of 15 kV, a beam current of 6 nA and a defocussed $10 \text{ }\mu\text{m}$ beam were used for glass shard analyses to minimise Na migration. The instrument was calibrated using a suite of mineral standards prior to analysis and secondary standards of ATHO-G, StHs6/80-G and GOR132-G were measured throughout analysis to monitor the system reproducibility and the precision and accuracy of glass analyses (secondary standard data are listed in Supplementary Table S.11). All major element concentrations have been normalised to an anhydrous basis.

Trace-elements were measured for the same glass shards using laser ablation inductively-coupled plasma mass spectrometry (LA-ICP-MS) at the Department of Geography and Earth Sciences, Aberystwyth University. The system comprises a Coherent Geolas 193 nm Excimer laser with a Thermo Finnigan Element 2 high-resolution sector field mass spectrometer (Pearce et al., 2007; 2011). Depending upon shard size, either a $10 \text{ }\mu\text{m}$ or $20 \text{ }\mu\text{m}$ diameter beam was used to ablate the shards at a laser energy of 10 J cm^{-2} , at a pulse rate of 5 Hz and with an acquisition time of 24 s. Trace element concentrations were calculated using the method of Perkins and Pearce (1995) and Pearce et al. (2007). NIST SRM 612 silicate glass was used as the calibration standard relative to concentrations from Pearce et al. (1997), and ATHO-G reference glass (Jochum et al., 2006) was used as a secondary standard during each run (listed in Supplementary Table S.12). ^{29}Si was used as an internal standard, determined from the same shards using EPMA and normalised to an anhydrous basis.

Comparison of the tephra chemistry with previously published data (Westgate and Evans, 1978; Busacca et al., 1992; Gaylord et al., 2001; Kuehn et al., 2009) using a similarity coefficient (Borchardt et al., 1972) indicates that the horizon sampled at Blackman Ridge Road (BRRMAZ) is the Mazama tephra, and also that the horizon sampled at McFeeley Road (MFRGP) is the Glacier Peak tephra (Figure 6; Supplementary Tables S.9-12). Although material sampled from MFRGP has previously been assigned to layer B of this tephra (Spencer and Knapp, 2010; Kuehn et al., 2009), our sample has greater chemical similarity with layer G (Table S.12). This may reflect sampling of a different part of this thick (>30 cm) horizon and does not affect this horizon's use as a geochronological marker because the ages of layers B and G are indistinguishable. Both the Mazama and Glacier Peak tephra horizons have robust age estimations from independent dating techniques and provide ideal independent age control in this investigation of fading-correction.

[Figure 6].

4.2.3 Luminescence sample preparation & measurement

Details of the preparation, luminescence and environmental dose rate measurement of polymineral fine-grained samples GOS3, GOS4, ZEL4 and ZEL7 are given in Preusser (1999, 2001) and Lowick et al. (2012). Samples 205/BRR-2, 204/MFRB-1 and 204/MFRB-2 were prepared using standard methods for polymineral fine grains at the Aberystwyth Luminescence Research Laboratory. All samples were treated with a 10 % v.v. dilution of HCl to remove carbonates, and 20 % H₂O₂ to remove organic material. The 4-11 µm grain size was isolated using Stokes' Law, and settling in 0.01 N sodium oxalate. Samples were measured using 0.98 cm diameter aluminium discs, and 1 mg of sample material was deposited from suspension in acetone onto each disc. Luminescence measurements were done using a Risø TL/OSL reader (Bøtter-Jensen et al., 2003) equipped with a 1.48 GBq ⁹⁰Sr/⁹⁰Y beta source and an EMI 9235QA photomultiplier. The radiation dose rate of the reader was 0.08 Gy s⁻¹ and IR stimulation used diodes emitting at 870 nm, with irradiance of ~135 mW cm⁻² when set at 90 %. The thermocouple of the instrument was checked prior to measurement, and no deviation between programmed and measured temperatures was recorded. Detection was restricted to the blue region using a 4 mm Corning 7-59, a 3 mm Schott GG-400 and a 2 mm BG-39 filter, giving a detection range of 400-500 nm. All measurements were made using a post-IR IRSL₂₂₅ measurement protocol which was selected using preheat plateau and dose-recovery preheat plateau experiments (cf. Roberts, 2012). Signals were integrated over the first 4 s, and backgrounds taken from the final 20 s of stimulation. All measured aliquots fulfilled the acceptance criteria of 1) aliquot recycling within 10 % of unity; 2) maximum equivalent dose

uncertainty <10 %; 3) maximum test dose signal (T_x) uncertainty <10 %, 4) signal $>3\sigma$ about background, 5) recuperation <5 %.

Fading was measured using a short-stimulation protocol (method 'b' of Huntley and Lamothe, 2001), and aliquots were preconditioned through multiple dose stimulation cycles prior to measurement. Aliquots were preheated immediately following dosing (Auclair et al., 2003). The IRSL₅₀ measurements were not made within a post-IR IRSL protocol, but rather in a protocol comprising only IRSL₅₀ stimulations, to facilitate measurement using a short optical stimulation of 0.38 s. An additional 'témoins' aliquot was measured to provide a control for signal loss due to successive signal bleaching (Huntley and Lamothe, 2001). The maximum delay was 39 days, fading rates for all samples are listed in Table 2. Raw measurement data are available in the Supplementary Material.

The environmental dose rate of the samples was calculated using DRAC v.1.2 (Durcan et al., 2015) using a combination of in-situ gamma spectrometry, thick-source alpha and beta counting (full details of the calculations are given in the Supplementary Material Tables S.13 and S.14). The conversion factors of Guérin et al. (2011) were used together with the beta grain size attenuation factors of Mejdahl (1979) and alpha grain size attenuation factors of Bell (1980). Water content was estimated at 10 ± 5 % for all samples and an alpha efficiency value of 0.0860 ± 0.0038 was assumed (Rees-Jones, 1995).

4.2.4 Comparison with independent age control

The IRSL₅₀ ages of all samples were fading-corrected using the Huntley (2006) model implemented with both a single-saturating exponential (1EXP, Kars et al., 2008) and general order kinetic fit (GOK, Guralnik et al., 2015a) as well as the approach of Huntley and Lamothe (2001); note that the Huntley and Lamothe (2001) fading correction was only applied to D_e values determined with a 1EXP fit. The details of these samples are summarised in Tables 2 and 3, and the results of the fading-correction relative to independent age control are shown in Figure 5. It was not possible to run the Huntley et al. (2006) model with a GOK fit for samples GOS4 or ZEL4 because the dose response curves are not sufficiently constrained; the uncertainty of the kinetic order, α , of sample ZEL7 is extremely high for the same reason (Table 3). It is immediately apparent that for all samples, the Huntley and Lamothe (2001) approach yields the youngest ages, whilst with the exception of GOS3, the Huntley (2006) model implemented with 1EXP yields the oldest ages, although almost all of the ages are within 2σ uncertainty. All three fading-correction approaches yield ages consistent with independent age control for samples GOS4, 204/MFRB-1 and 205/BRR-2, whilst the 1EXP implementation of the Huntley (2006) model overestimates age for sample 204/MFRB-2. However, whereas the

Huntley and Lamothe (2001) fading corrected ages are within 2σ uncertainties of independent ages for samples GOS3 and ZEL4, the Huntley (2006) fading corrected ages overestimate the independent age of these samples. The greatest age discrepancy is recorded for sample ZEL7, however the exact location of this sample relative to the independent age control is unclear (Figure 5).

It is promising that the performance of the Huntley (2006) model using either the 1EXP or GOK approach is similar to that of the Huntley and Lamothe (2001) model, although the lower ages obtained using the latter approach may relate to its application beyond the linear part of the dose response curve. However, the age discrepancies between the 1EXP and GOK implementations of the Huntley (2006) model are concerning. A potential explanation for this may relate to constraint of dose response during laboratory measurements, which especially for younger samples may not characterise the complete dose response curve. Applying the Huntley (2006) model involves interpolating the measured natural luminescence signal (L_{nat}) onto a simulated natural dose response curve (Kars et al., 2008) calculated using the unfaded D_0 value, fading rate and kinetic order (α), if a GOK fit is used. To explore the effect of changing dose response curve constraint on calculated age, we used the measurement data of samples 204/MFRB-1, 204/MFRB-2 and 205/BRR-2, which were dosed until saturation (i.e. using a maximum regenerative dose of 4.7 kGy). Starting with a dataset that allowed interpolation of L_{nat} between at least two regenerative dose points, we progressively re-fitted the data including additional regenerative doses of 147 Gy, 295 Gy, 590 Gy, 2358 Gy and 4717 Gy with the `calc_Huntley2006()` function using either a 1EXP or GOK fit to calculate age (Figure 7).

All samples exhibited similar behaviour; in contrast to the 1EXP fit, 590 Gy was the lowest, maximum regenerative dose value that could be fitted using a GOK fit for these samples. With increasing regenerative doses, D_e values determined using a 1EXP fit increased by 13-16% (i.e. 7 Gy for sample MFRB2), whereas those determined using a GOK fit increased by only 2-4% (Figure 7A). The characteristic dose of saturation (D_0) increased by 50-60% with the inclusion of greater regenerative doses for 1EXP, but reduced by 35-64% for the GOK fit (Figure 7B). Estimation of $(n/N)_{ss}$ reduced by only 2-4% for either fit, whereas (n/N) values reduced by 43-52% for 1EXP and increased by 35-60% for the GOK fitting (Figure 7C). Huntley (2006) model fading corrected ages calculated with 1EXP increased by 20-24% (i.e. 4 ka for sample 204/MFRB-2), whereas those calculated with GOK exhibited a reduction of 2%. The Huntley and Lamothe (2001) model fading corrected ages, calculated using D_e values determined from a 1EXP fit, exhibited an increase of 13-16% following the increase in D_e values (Figure 7A, Figure 7D). In contrast where D_e values determined from a GOK fit were used, Huntley and Lamothe (2001) model fading corrected ages increased by only 2-4% (Figure 7A, Figure 7D).

Sample 204/MFRB-2 has the most robust independent age control, as it directly overlies the Glacier Peak tephra, which has known depositional age of 13.5 ± 0.1 cal. ka BP (Kuehn et al., 2009) and we focus on this sample to determine the implications of our results. Whereas an age overestimation is obtained when all of the regenerative data are fitted with the Huntley (2006) model and 1EXP (17.1 ± 1.4 ka), fewer regenerative doses yield ages within uncertainty of the independent age (Figure 7D), however a clear trend of increasing age with increasing regenerative dose is apparent. In contrast the Huntley (2006) and GOK fading corrected ages are commensurate with the independent age control for all regenerative dose combinations, reducing by 2% with increasing regenerative dose (Figure 7D). The key difference between the two implementations of the Huntley (2006) model is the form of the dose response curve that L_{nat} is interpolated on.

Kars et al. (2008) assumed that the luminescence dose response of feldspar followed a single saturating exponential, and this implementation has been used in a number of studies (e.g. King et al., 2016a,b; Li et al., 2017). However for some samples, feldspar luminescence dose response can be better fitted using a GOK (e.g. Guralnik et al., 2015a,b; Li et al., 2018) or double saturating exponential function (e.g. Buylaert et al., 2012; Li et al., 2015), which is also true for the three samples investigated here (e.g. 204/MFRB-2, Figure 8A). Whereas either a GOK fit or a double exponential fit passes through all of the data-points, the 1EXP fit exhibits clear bias, overestimating dose at low doses and underestimating dose at high doses (Figure 8B). The improved fit of a double exponential or GOK curve is clearly demonstrated when the impact of fitting increasingly high dose, dose response data is explored (Figure 7A). In contrast to the 16% variation in D_e values recorded for the single saturating exponential fit, the D_e values obtained from the double saturating exponential fit or GOK fit vary by only 0-4% (Figure 7A). Thus the Huntley (2006) and 1EXP approach seems to be affected by interpolation of the natural signal (L_{nat}) onto a simulated natural dose response curve of inappropriate form.

The investigations presented here indicate that the Huntley (2006) model implemented with a GOK fit is most appropriate for sample fading correction, and this approach has been used previously (Guralnik et al., 2015b; Valla et al., 2016; Lambert et al., In Revision) however a number of caveats remain for its use. First it is only possible to fit well characterised dose response curves, as demonstrated by the model failure to determine finite ages for samples GOS4 and ZEL4. Whilst it was possible to fit sample GOS3, which has a maximum regenerative dose of only 210 Gy, it was not possible to fit the dose response data of a number of samples from Valla et al. (2016) where the maximum regenerative dose was 2.5 kGy, which is partly related to the very high rates of fading for these samples. Samples 204/MFRB-1, 204/MFRB-2 and 205/BRR-2 could only be fitted where a maximum regenerative dose of ~ 600 Gy or greater was used, and thus we tentatively propose this as a minimum threshold, but note that this will

be sample specific. Secondly the GOK implementation of the Huntley et al. (2006) model yielded less accurate (n/N) values for samples known to be in field saturation (Figure 4) than the 1EXP model implementation. Little difference in $(n/N)_{ss}$ was recorded between the two fitting methods (Figure 7C), and this may indicate that the GOK implementation performs less well for samples that interpolate further along the dose response curve, however we are unable to test this within the present study. Finally, and related to the former point, it is unknown whether laboratory feldspar dose response always mimics the form of natural dose response. Previous studies on the luminescence and electron spin resonance of quartz have revealed markedly different laboratory behaviour in comparison to naturally accumulated signals (Chapot et al., 2012; Timar-Gabor et al., 2015; Tsukamoto et al., In Revision), and it seems reasonable that some feldspar may behave similarly. However, Li and Li (2012) constructed a natural luminescence dose response curve for K-feldspar extracted from loess at Luochuan, China. Using the independent age control at this site, they found that natural dose response for multiple-elevated temperature luminescence measurements followed a single saturating exponential. Furthermore for these samples laboratory generated dose response curves also exhibited similar form. Further studies on feldspar of different origins and chemical compositions are required to confirm whether laboratory dose response always mimics natural dose response, and also whether this is true for all measurement protocols. Despite these limitations, the performance of the Huntley (2006) model implemented with GOK seems to be appropriate for feldspar fading age correction, whilst using a 1EXP fit may result in a slight bias towards age overestimation (Figure 7); we also note that other curve forms may yield accurate fading corrected ages, providing that they fit the measured data adequately.

[Figure 8]

5. Threshold values: What does $2D_0$ mean for feldspar?

Wintle and Murray (2006) proposed an upper D_e interpolation value of $2D_0$ for the derivation of finite age estimates from quartz. Beyond this threshold, which is equivalent to 86 % of saturation, interpolation of L_{nat} results in a large uncertainty because of the relatively small rate of change (per unit dose) in the dose response curve. In contrast, below this threshold, luminescence signals are often regarded as finite. However the validity of applying this threshold to feldspar data remains questionable unless anomalous fading has been corrected for, because fading can cause a saturated sample to have $D_e < 2D_0$ resulting in misidentification of a saturated sample, as a sample of finite age.

For a non-fading sample, the laboratory and natural dose response curves are considered to be equivalent (although see for example the discussion in Chapot et al., 2012). In contrast, for a sample which is affected by time-dependent athermal signal loss (i.e. anomalous fading) the laboratory dose response and natural dose response curves are not equivalent, because of the different time periods over which dose accumulates; this is shown in Figure 3. Because the laboratory dose response curve accumulates over a very short time period a much greater amount of charge can be stored and the dose response curve is able to grow to a greater level of saturation than would be possible in nature. In contrast, the natural dose response curve for the IRSL₅₀ signal of sample NB124 (as simulated using the `calc_Huntley2006()` function) reaches a much lower level of saturation, with $(n/N)_{ss}$ of $38 \pm 5 \%$ (Figure 3). The difference between the laboratory and natural dose response curves is greatest for the samples that fade most, and thus post-IR IRSL₂₂₅ and post-IRSL₂₉₀ signals, which fade least, may not be affected. The consequence of this mismatch between the laboratory and natural dose response curves means that the notion of $D_e < 2D_0$ as a threshold for feldspar signal saturation is not applicable to feldspars which experience anomalous fading, unless this fading is corrected.

To illustrate this effect graphically, the equivalent of the laboratory-measured saturation ratio $(L_{nat})/(L_{labmax})$ for a continuum of synthetic saturated samples was computed using the Huntley (2006) model with 1EXP for g_{2days} values ranging from 0 % to 30 %/decade (Figure 9). We chose to use 1EXP rather than GOK because of the improved performance of 1EXP in Figure 4, but both fits would yield similar results. This calculation comprised three stages: (i) $(n/N)_{ss}$ was computed based on an unfaded D_0 of 400 Gy, \dot{D} of 5 Gy ka⁻¹, and ρ' values of 0 to 1.65×10^{-5} (approximately equal to g_{2days} of 0 % to 30 %/decade). (ii) Fading over laboratory timescales means that the maximum measured light intensity (L_{labmax}) is lower than would be measured for a non-fading sample. This can be seen through the difference between the measured and simulated unfaded dose response curves in Figure 3. The level of laboratory saturation (N_{lab}/N) achievable for a given sample can be calculated using the same approach as in stage (i), but substituting the environmental dose rate for \dot{D}_{lab} , which in this calculation was set to 0.134 Gy s⁻¹. (iii) Once (N_{lab}/N) has been calculated, it is possible to derive the equivalent laboratory measured saturation ratio, $(L_{nat})/(L_{labmax})$ where L_{nat} is the sensitivity corrected natural luminescence signal and L_{labmax} is the maximum light level measured in the laboratory, equivalent to the maximum possible L_x/T_x measurement for that specific sample under the same experimental conditions. $(L_{nat})/(L_{labmax})$ can thus be derived from $1/(N_{lab}/N) * (n/N)_{ss}$.

The modelled relationship between $(L_{nat})/(L_{labmax})$ and g_{2days} is validated through comparison with the previously published $(L_{nat})/(L_{labmax})$ values (Table 1) for 50 published samples reported to be in field saturation, across a range of different signals (IRSL₅₀, post-IR

IRSL_{100/150/225/290}) (Figure 9). It is apparent that fading rate must be considered when evaluating whether a sample is in saturation (cf. Valla et al., 2016). The importance of this can be particularly illustrated through considering that a sample with g_{2days} of 3.77 %/decade in field saturation has $(L_{nat})/(L_{labmax})$ that interpolates onto the laboratory dose response curve at $1D_0$ (Figure 9). Applying the $2D_0$ criterion to this sample would result in it being mistakenly interpreted as having a finite age.

[Figure 9]

5. Conclusions

Anomalous fading remains challenging for luminescence dating of feldspars. Using a new **R** function that is freely available in the 'Luminescence' package (v.0.8.1) and through comparison of a suite of samples with independent age control from radiocarbon dating, $^{230}\text{Th}/\text{U}$ TIMS and tephrochronology, we show that the model of Huntley (2006) implemented with a general order kinetic fit (Guralnik et al., 2015a) is appropriate for sample fading correction. Implementing the Huntley (2006) model with a single saturating exponential fit following Kars et al. (2008) results in age overestimation for the samples investigated in this study, because their luminescence dose response is not well described by this form. If a general order kinetic fit is used, sample dose response curves must include a maximum regenerative dose that is greater than ~600 Gy, otherwise a robust fit is not obtained. We also tested the performance of the Huntley (2006) model for determining sample saturation through applying it to a set of saturated samples from literature, the model implemented with a single saturating exponential fit performed best, yielding an accuracy of ~10 %. In contrast using a general order kinetic fit performed less well, possibly indicating that feldspar do not follow this form of natural dose response in nature. Further research is required to investigate the form of feldspar natural dose response in comparison to that obtained using laboratory measurements.

Acknowledgements

Sally Lowick is thanked for providing the raw data files for sample GOS3, GOS4, ZEL4 and ZEL7. Mark Sweeney and David Gaylord are thanked for help sampling McFeeley Road and Blackman Ridge Road, and Victoria Smith for assistance with acquiring the geochemical data. Benny Guralnik and Frédéric Herman are gratefully acknowledged for useful discussions. GEK acknowledges support from the Climate Change Consortium of Wales (C3W) and Swiss National Science Foundation (SNSF) grant number PZ00P2-167960. The manuscript benefitted from the comments of Sumiko Tsukamoto and another anonymous reviewer.

References

- 540 Aitken, M.J., 1985. Thermoluminescence dating. Academic press.
- 541 Andersen, M.T., Jain, M., Tidemand-Lichtenberg, P., 2012. Red-IR stimulated luminescence in K-feldspar: Single or multiple trap
- 542 origin?. *Journal of Applied Physics*. 5;112(4):043507.
- 543 Auclair, M., Lamothe, M., and Huot, S., 2003. Measurement of anomalous fading for feldspar IRSL using SAR. *Radiation*
- 544 *measurements* 37(4), 487-492.
- 545 Auclair, M., Lamothe, M., Lacroix, F., Banerjee, S.K., 2007. Luminescence investigations of loess and tephra from Halfway House
- 546 section, Central Alaska. *Quaternary Geochronology* 2, 34-38.
- 547 Bell, W.T., 1980. Alpha attenuation in Quartz grains for Thermoluminescence Dating. *Ancient TL* 12, 4-8.
- 548 Berger, A.L., Spotila, J.A., Chapman, J.B., Pavlis, T.L., Enkelmann, E., Ruppert, N.A. and Buscher, J.T., 2008. Architecture, kinematics,
- 549 and exhumation of a convergent orogenic wedge: a thermochronological investigation of tectonic-climatic interactions within
- 550 the central St. Elias Orogen, Alaska. *Earth Planetary Science Letters* 270, 13-24.
- 551 Bickel, L., Lüthgens, C., Lomax, J. and Fiebig, M., 2015. Luminescence dating of glaciofluvial deposits linked to the penultimate
- 552 glaciation in the Eastern Alps. *Quaternary International* 357, 110-124.
- 553 Borchardt, G.A., Aruscavage, P.J. and Millard Jr, H.T., 1972. Correlation of the Bishop Ash, a Pleistocene marker bed, using
- 554 instrumental neutron activation analysis. *Journal of Sedimentary Research* 42(2), 301-306.
- 555 Bøtter-Jensen, L., Andersen, C.E., Duller, G.A.T. and Murray, A.S., 2003. Developments in radiation, stimulation and observation
- 556 facilities in luminescence measurements. *Radiation Measurements* 37, 535-541.
- 557 Busacca, A.J., Nelstead, K.T., McDonald, E.V. and Purser, M.D., 1992. Correlation of distal tephra layers in loess in the Channeled
- 558 Scabland and Palouse of Washington State. *Quaternary Research* 37(3), 281-303.
- 559 Buylaert, J.P., Murray, A.S. and Huot, S., 2008. Optical dating of an Eemian site in Northern Russia using K-feldspar Radiation
- 560 *Measurements* 43(2-6), 715-720
- 561 Buylaert, J.P., Murray, A.S., Thomsen, K.J., and Jain, M., 2009. Testing the potential of an elevated temperature IRSL signal from K-
- 562 feldspar. *Radiation Measurements* 44(5), 560-565.
- 563 Buylaert J.P., Jain M., Murray, A.S., Thomsen, K.J., Thiel, C. and Sohbat, R., 2012. A robust feldspar luminescence dating method for
- 564 Middle and Late Pleistocene sediments. *Boreas* 41, 435-451.
- 565 Chapot, M.S., Roberts, H.M., Duller, G.A.T., and Lai, Z.P., 2012. A comparison of natural-and laboratory-generated dose response
- 566 curves for quartz optically stimulated luminescence signals from Chinese Loess. *Radiation Measurements* 47(11), 1045-1052.
- 567 Diaz, N., King, G.E., Valla, P.G., Herman, F., and Verrecchia, E.P., 2016. Pedogenic carbonate nodules as soil time archives: Challenges
- 568 and investigations related to OSL dating. *Quaternary Geochronology* 36, 120-133.
- 569 Durcan, J.A., King, G.E. and Duller, G.A.T., 2015. DRAC: Dose Rate and Age Calculator for trapped charge dating. *Quaternary*
- 570 *Geochronology* 28, 54-61.
- 571 Gaylord, D.R., Foit, F.F., Schatz, J.K. and Coleman, A.J., 2001. Smith Canyon dune field, Washington, USA: relation to glacial outburst
- 572 floods, the Mazama eruption, and Holocene paleoclimate. *Journal of arid environments* 47(4), 403-424.
- 573 Geyh, M.A., Hennig, G. and Oetzen, D. 1997. U/Th-Datierung interglazialer und interstadialer Niedermoortorfe und Lignite: Stand
- 574 und Zukunft. *Schriftenreihe der Deutschen Geologischen Gesellschaft* 4, 187-199.
- 575 Geyh, M.A. and Schlüchter, C., 1998. Zur Kalibration der ¹⁴C Zeitskala vor 22,000 Jahren. *v.h. GeoArchaeoRhein* 2, 139-149.
- 576 Guerin, G., Mercier, N., Adamiec, G., 2011. Dose-rate conversion factors: update. *Ancient TL*, 29, 5-8.
- 577 Guralnik, B., Jain, M., Herman, F., Ankjærgaard, C., Murray, A.S., Valla, P.G., Preusser, F., King, G.E., Chen, R., Lowick, S.E. and Kook, M.,
- 578 2015a. OSL-thermochronometry of feldspar from the KTB borehole, Germany. *Earth and planetary science letters* 423, 232-243.
- 579 Guralnik, B., Li, B., Jain, M., Chen, R., Paris, R.B., Murray, A.S., Li, S.H., Pagonis, V., Valla, P.G. and Herman, F., 2015b. Radiation-induced
- 580 growth and isothermal decay of infrared-stimulated luminescence from feldspar. *Radiation Measurements*, 81, pp.224-231.
- 581 Hendriks, B., Andriessen, P., Huigen, Y., Leighton, C., Redfield, T., Murrell, G., Gallagher, K. and Nielsen, S.B., 2007. A fission track data
- 582 compilation for Fennoscandia. *Norwegian Journal of Geology* 87, 143-155.
- 583 Huntley, D.J., and Lamothe, M., 2001. Ubiquity of anomalous fading in K-feldspars and the measurement and correction for it in
- 584 optical dating. *Canadian Journal of Earth Sciences* 38(7), 1093-1106.
- 585 Huntley, D.J. and Lian, O.B., 2006. Some observations on tunneling of trapped electrons in feldspars and their implications for
- 586 optical dating. *Quaternary Science Reviews* 25, 2503-2512.
- 587 Huntley, D.J., 2006. An explanation of the power-law decay of luminescence. *Journal of Physics: Condensed Matter* 18(4), 1359-1365.

- Jochum, K.P., Stoll, B., Herwig, K., Willbold, M., Hofmann, A.W., Amini, M., Aarburg, S., Abouchami, W., Hellebrand, E., Mocek, B., Raczek, I., Stracke, A., Alard, O., Bouman, C., Becker, S., Dücking, M., Brätz, H., Klemd, R., de Bruin, D., Canil, D., Cornell, D., de Hoog, C., Dalpé, C., Danyushevsky, L., Eisenhauer, A., Gao, Y., Snow, J.E., Groschopf, N., Günther, D., Latkoczy, C., Guillong, M., Hauri, E., Höfer, H.E., Lahaye, Y., Horz, K., Jacob, D.E., Kasemann, S.A., Kent, A.J.R., Ludwig, T., Zack, T., Mason, P.R.D., Meixner, A., Rosner, M., Misawa, K., Nash, B.P., Pfänder, J., Premo, W.R., Sun, W.D., Tiepolo, M., Vannucci, R., Vennemann, T., Wayne, D., Woodhead, J.D., (2006). MPI-DING reference glasses for in situ microanalysis: new reference values for element concentrations and isotope ratios. *Geochemistry Geophysics Geosystems* 7, Q02008.
- Kars, R.H., Wallinga, J., and Cohen, K.M., 2008. A new approach towards anomalous fading-correction for feldspar IRSL dating-tests on samples in field saturation. *Radiation Measurements* 43(2), 786-790.
- Kars, R.H. and Wallinga, J., 2009. IRSL dating of K-feldspars: Modelling natural dose response curves to deal with anomalous fading and trap competition. *Radiation Measurements* 44(5), 594-599.
- Kars, R.H., Reimann, T., Ankjærgaard, C., and Wallinga, J., 2014. Bleaching of the post-IR IRSL signal: new insights for feldspar luminescence dating. *Boreas* 43(4), 780-791.
- King, G.E., Herman, F., Lambert, R., Valla, P.G. and Guralnik, B., 2016a. Multi-OSL-thermochronometry of feldspar. *Quaternary Geochronology* 33, 76-87.
- King, G.E., Herman, F., and Guralnik, B., 2016b. Northward migration of the eastern Himalayan syntaxis revealed by OSL thermochronometry. *Science* 353(6301), 800-804.
- King, G.E., Pearce, N.J.G., Westgate, J., Smith, V.C., Roberts, H.M., Gaylord, D.R., Sweeney, M., 2016c. Identification of Kulshan caldera tephra, Palouse Loess, Washington State, USA. *Quaternary Research* 86(2), 232-241.
- King, G.E., Guralnik, B., Valla, P.G. and Herman, F., 2016d. Trapped-charge thermochronometry and thermometry: A status review. *Chemical Geology*, 446, 3-17.
- King, G., Burow, C. (2018). `calc_Huntley2006()`: Apply the Huntley (2006) model. Function version 0.4.0. In: Kreutzer, S., Burow, C., Dietze, M., Fuchs, M.C., Schmidt, C., Fischer, M., Friedrich, J. (2018). *Luminescence: Comprehensive Luminescence Dating Data Analysis*. R package version 0.8.1. <https://CRAN.R-project.org/package=Luminescence>
- Kreutzer, S., Schmidt, C., Fuchs, M.C., Dietze, M., Fischer, M. and Fuchs, M., 2012. Introducing an R package for luminescence dating analysis. *Ancient TL* 30(1), 1-8.
- Kreutzer, S., Burow, C., Dietze, M., Fuchs, M.C., Schmidt, C., Fischer, M. and Friedrich, J., 2018. *Luminescence: Comprehensive Luminescence Dating Data Analysis*. R package version 0.8.1. <https://CRAN.R-project.org/package=Luminescence>
- Kreutzer, S. and Burow, C., 2017. `analyse_FadingMeasurement()`: Analyse fading measurements and returns the fading rate per decade (g-value). Function version 0.1.1. In: Kreutzer, S., Dietze, M., Burow, C., Fuchs, M.C., Schmidt, C., Fischer, M. and Friedrich, J., 2017. *Luminescence: Comprehensive Luminescence Dating Data Analysis*. R package version 0.7.4. <https://CRAN.R-project.org/package=Luminescence>
- Kuehn, S.C., Froese, D.G., Carrara, P.E., Foit, F.F., Pearce, N.J. and Rotheisler, P., 2009. Major-and trace-element characterization, expanded distribution, and a new chronology for the latest Pleistocene Glacier Peak tephra in western North America. *Quaternary Research* 71(2), 201-216.
- Lamothe, M. and Auclair, M., 1999. A solution to anomalous fading and age shortfalls in optical dating of feldspar minerals. *Earth and Planetary Science Letters* 171, 319-323.
- Lamothe, M. and Auclair, M., 2000. The fadia method: a new approach in luminescence dating using the analysis of single feldspar grains. *Radiation Measurements* 32(5-6), 2000.
- Lamothe, M., Auclair, M., Hamzaoui, C., and Huot, S., 2003. Towards a prediction of long-term anomalous fading of feldspar IRSL. *Radiation Measurements* 37(4), 493-498.
- Lambert, R., King, G.E., Valla, P.G., Herman, F., In Revision. Investigating thermal kinetic processes of feldspar for the application of luminescence thermochronometry. *Radiation Measurements*.
- Lauer, T., Vlaminc, S., Frechen, M., Rolf, C., Kehl, M., Sharifi, J., Lehndorff, E. and Khormali, F., 2017. The Agh Band loess-palaeosol sequence – A terrestrial archive for climatic shifts during the last and penultimate glacial-interglacial cycles in a semiarid region in northern Iran. *Quaternary International*, 429, 13-30.
- Li, B. and Li, S.H., 2008. Investigations of the dose-dependent anomalous fading rate of feldspar from sediments. *Journal of Physics D: Applied Physics* 41(22) 225502, 15.
- Li, B., and Li, S.H., 2011. Luminescence dating of K-feldspar from sediments: a protocol without anomalous fading-correction. *Quaternary Geochronology* 6(5), 468-479.
- Li, B. and Li, S.H., 2012. Luminescence dating of Chinese loess beyond 130 ka using the non-fading signal from K-feldspar. *Quaternary Geochronology*, 10, 24-31.

- Li, B., Jacobs, Z., Roberts, R.G., Li, S.H., 2018. Single-grain dating of potassium-rich feldspar grains: Towards a global standardized growth curve for the post-IR IRSL signal. *Quaternary Geochronology* 45, 23-36.
- Li, Y., Tsukamoto, S., Frechen, M., Gabriel, G., 2018. Timing of fluvial sedimentation in the Upper Rhine Graben since the middle Pleistocene: constraints from quartz and feldspar luminescence dating. *Boreas* 47(1), 256-270.
- Lowick, S.E., Trauerstein, M. and Preusser, F., 2012. Testing the application of post IR-IRSL dating to fine grain waterlain sediments. *Quaternary Geochronology* 8, 33-40.
- Mejdahl, V., 1979. Thermoluminescence Dating: Beta-Dose Attenuation in Quartz Grains. *Archaeometry* 21, 61-72.
- Mochanov, Yu. A., 1988. The most ancient Paleolithic of the Diring and the problem of a nontropical origin of humanity. In: Alekseev, A.N., Ivanova, L.T., Kochmar, N.N., (Eds.), *Archaeology of Yakutia*. Yakutsk State University, pp. 15-54 (English translation: *Arctic Anthropology* 30, 22-53, 1993).
- Morthekai, P., Jain, M., Cunha, P.P., Azevedo, J.M. and Singhvi, A.K., 2011. An attempt to correct for the fading in million year old basaltic rocks. *Geochronometria* 38(3), 223-230.
- Nielsen, S.B., Gallagher, K., Leighton, C., Balling, N., Svenningsen, L., Jacobsen, B.H., Thomsen, E., Nielsen, O.B., Heilmann-Clausen, C., Egholm, D.L., Summerfield, M.A., Clausen, O.R., Piotrowski, J.A., Thorsen, M.R., Huuse, M., Abrahamsen, N., King, C. and Lykke-Andersen, H., 2009. The evolution of western Scandinavian topography: a review of Neogene uplift versus the ICE (isostasy-climate-erosion) hypothesis. *Journal of Geodynamics* 47, 72-95.
- Pearce N.J.G., Denton J.S., Perkins W.T., Westgate J.A. and Alloway B.V., 2007. Correlation and characterisation of individual glass shards from tephra deposits using trace element laser ablation ICP-MS analyses: current status and future potential. *Journal of Quaternary Science*, 22, 721-736.
- Pearce N.J.G., Perkins W.T. Westgate J.A. and Wade S.C., 2011. Trace element analysis by laser ablation ICP-MS: the quest for comprehensive chemical characterisation of single sub-10um volcanic glass shards. *Quaternary International*, 246, 57-81.
- Pearce N.J.G., Perkins W.T., Westgate J.A., Gorton M.P., Jackson S.E., Neal C.R. and Chenery S.P., 1997. A compilation of new and published major and trace element data for NIST SRM 610 and NIST SRM 612 glass reference materials. *Geostandards Newsletter*, 21, 115-144.
- Perkins W.T. and Pearce N.J.G., 1995. Mineral microanalysis by laserprobe inductively coupled plasma mass spectrometry. In Potts P.J., Bowles J.F.W., Reed S.J.B. and Cave M.R. (Editors) "Microprobe Techniques in the Earth Sciences", The Mineralogical Society, 291-325.
- Preusser, F., 1999. Luminescence dating of fluvial sediments and overbank deposits from Gossau, Switzerland: fine grain dating. *Quaternary Science Reviews* 18(2), 217-222.
- Preusser, F., Muller, B.U. and Schlüchter, C., 2001. Luminescence dating of sediments from the Luthern Valley, central Switzerland, and implications for the chronology of the last glacial cycle. *Quaternary Research* 55, 215-222.
- Preusser, F., 2003. IRSL dating of K-rich feldspars using the SAR protocol: comparison with independent age control. *Ancient TL* 21(1), 17-23.
- Rees-Jones, J., 1995. Optical Dating of young Sediments using Fine-Grain Quartz. *Ancient TL* 13(2), 9-14.
- Reimann, T. and Tsukamoto, S., 2012. Dating the recent past (< 500 years) by post-IR IRSL feldspar-Examples from the North Sea and Baltic Sea coast. *Quaternary Geochronology* 10, 180-187.
- Roberts, H.M., 2012. Testing Post-IR IRSL protocols for minimising fading in feldspars, using Alaskan loess with independent chronological control. *Radiation Measurements* 47, 716-724.
- Schlüchter, C., Maisch, M., Suter, J., Fitze, P., Keller, W.A., Burga, A. and Wynistorf, E., 1987. Das Schieferkohlen-Profil von Gossau (Kanton Zürich) und seine stratigraphische Stellung innerhalb der letzten Eiszeit. *Vierteljahrsschrift der Naturforschenden Gesellschaft in Zürich* 132/3, 135-174.
- Spencer, P.K. and Knapp, A.N., 2010. New stratigraphic markers in the late Pleistocene Palouse loess: novel fossil gastropods, absolute age constraints and non-aeolian facies. *Sedimentology* 57, 41-52.
- Spotila, J.A., Buscher, J.T., Meigs, A.J. and Reiners, P.W., 2004. Long-term glacial erosion of active mountain belts: Example of the Chugach-St. Elias Range, Alaska. *Geology* 32, 501-504.
- Thiel, C., Buylaert, J.P., Murray, A., Terhorst, B., Hofer, I., Tsukamoto, S. and Frechen, M., 2011. Luminescence dating of the Stratzing loess profile (Austria)-Testing the potential of an elevated temperature post-IR IRSL protocol. *Quaternary International* 234(1), 23-31.
- Thomsen, K.J., Murray, A.S., Jain, M., and Bøtter-Jensen, L., 2008. Laboratory fading rates of various luminescence signals from feldspar-rich sediment extracts. *Radiation measurements* 43(9), 1474-1486.

- 690 Thomsen, K.J., Murray, A.S. and Jain, M., 2011. Stability of IRSL signals from sedimentary K-feldspar
691 samples. *Geochronometria* 38(1), 1-13.
- 692 Timar-Gabor, A., Constantin, D., Buylaert, J. P., Jain, M., Murray, A. S., & Wintle, A. G. (2015). Fundamental investigations of natural
693 and laboratory generated SAR dose response curves for quartz OSL in the high dose range. *Radiation Measurements*, 81, 150-
694 156.
- 695 Tsukamoto, S., Long, H., Richter, M., Li, Y, King, G.E., Zhong, H., Yang, L., Zhang, J., In Revision. Quartz natural and laboratory ESR dose
696 response curves: A first attempt from Chinese loess. *Radiation Measurements*.
- 697 Valla, P.G., Lowick, S.E., Herman, F., Champagnac, J.D., Steer, P. and Guralnik, B., 2016. Exploring IRSL 50 fading variability in bedrock
698 feldspars and implications for OSL thermochronometry. *Quaternary Geochronology* 36, 55-66.
- 699 Wallinga, J., Bos, A.J., Dorenbos, P., Murray, A.S. and Schokker, J., 2007. A test case for anomalous fading correction in IRSL
700 dating. *Quaternary Geochronology*, 2(1), pp.216-221.
- 701 Westgate, J.A. and Evans, M.E., 1978. Compositional variability of Glacier Peak tephra and its stratigraphic significance. *Canadian*
702 *Journal of Earth Sciences* 15(10), 1554-1567.
- 703 Wintle, A.G. and Murray, A.S., 2006. A review of quartz optically stimulated luminescence characteristics and their relevance in
704 single-aliquot regeneration dating protocols. *Radiation Measurements* 41(4), 369-391.
- 705 Zdanowicz, C.M., Zielinski, G.A., Germani, M.S., 1999. Mount Mazama eruption: Calendrical age verified and atmospheric impact
706 assessed. *Geology* 27, 621-624.
- 707 Zhang, J., Tsukamoto, S., Nottebaum, V. and Lehmkuhl, F., 2015. De Plateau and its implications for post-IR IRSL dating of polymineral
708 fine grains. *Quaternary Geochronology* 30, 147-153.
- 709 Zeitler, P.K., Meltzer, A.S., Brown, L., Kidd, W.S., Lim, C. and Enkelmann, E., 2014. Tectonics and topographic evolution of Namche
710 Barwa and the easternmost Lhasa block, Tibet. *Geological Society of America Special Papers*, 507.

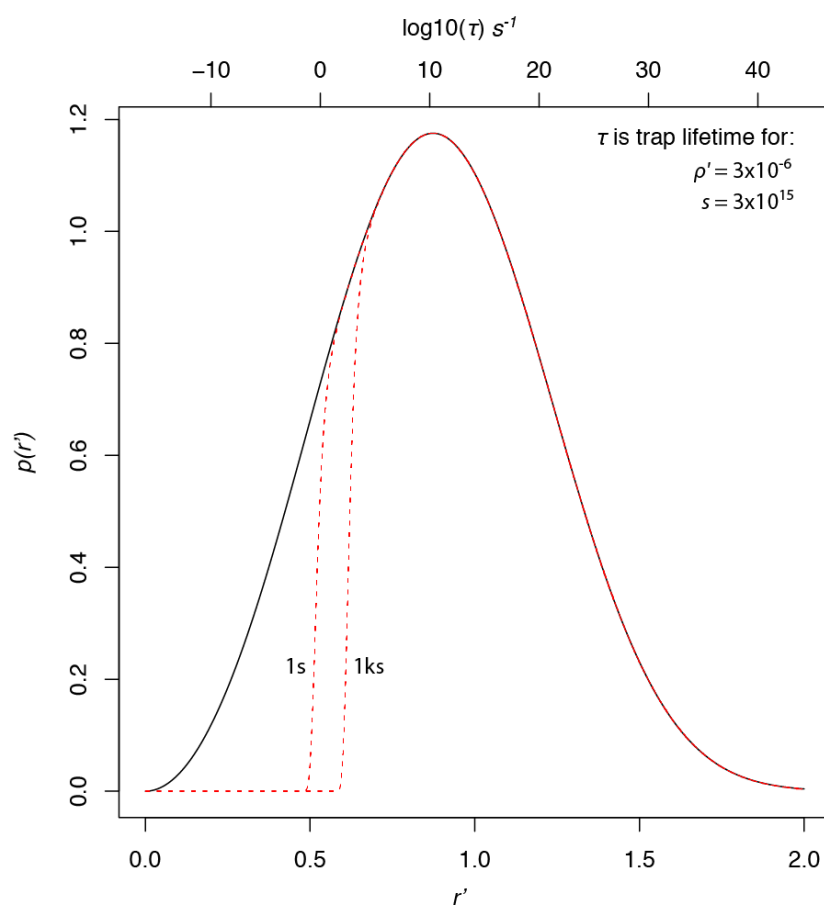


Figure 1: Probability distribution ($p(r')$) of dimensionless distances (r') between trapped electrons and recombination centres following Huntley (2006) for a given dimensionless density of recombination centres ($\rho' = 3 \times 10^{-6}$) after an instantaneous pulse of irradiation. The lifetime (τ) of an electron in a given trap increases with increasing distance between the trap and the recombination centre, thus trapped charge with nearby recombination centres (left-side of the figure) are unstable over laboratory timescales. The dashed red lines indicate the remaining trapped electron population after 1 s and 1 ks, i.e. following recombination of electrons in the most unstable traps.

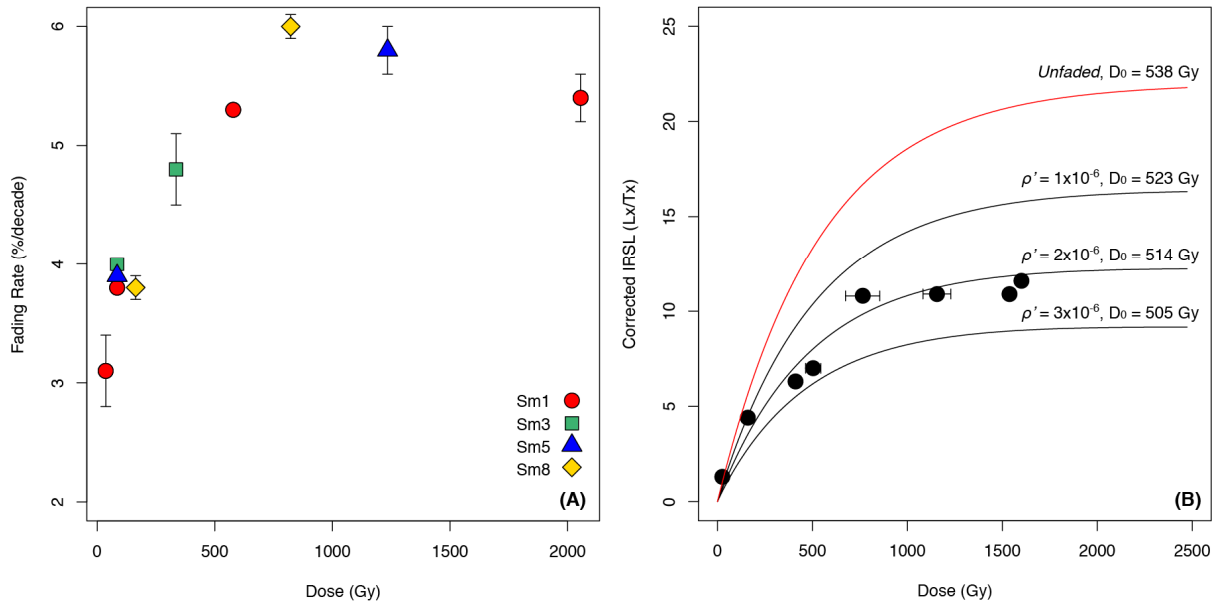


Figure 2: (A) Fading rate as a function of given dose, redrawn from Li and Li (2008, their Figure 11). (B) Natural luminescence signal intensities plotted against estimated palaeodose, contrasted with modelled dose response curves for different rates of athermal signal loss, redrawn from Li and Li (2008, their Figure 12a). Modelled dose response curves were calculated using an average environmental dose rate of 3.9 Gy/ka and equation: $\frac{Lx}{Tx}(t) = e^{-\rho' \ln(1.8 \tilde{s} t)^3} A (1 - e^{-\frac{D}{D_0}})$ (King et al., 2016a) where A is a constant scaling factor of 22, to match the original figure (Li and Li, 2008). Whereas the data in (A) suggest that the rate of sample fading will vary significantly with dose, in (B) it is apparent that the data are well described by a single saturating dose response curve computed based on a single density of recombination centres using the model of Huntley (2006).

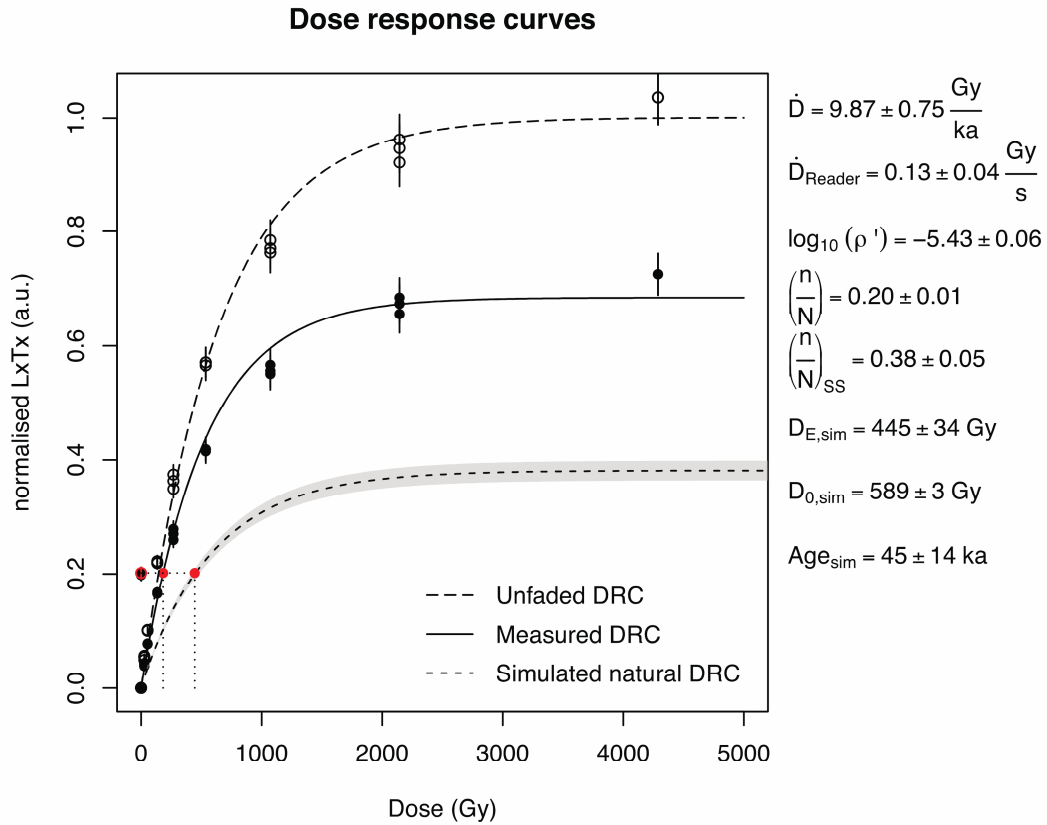


Figure 3: Laboratory measured, simulated unfaded, and simulated natural dose response curves for the IRSL_{50} signal of sample UNIL/NB124 (King et al., 2016a) output from the `calc_Huntley2006()` function of the **R** package ‘Luminescence’ (Kreutzer et al., 2012; 2018) fitted with a single-saturating exponential fit (following Kars et al., 2008). The simulated unfaded dose response curve is calculated using equation (1) after Kars et al. (2008), whereas the simulated natural dose response curve is calculated using the sample specific \dot{D} : $9.87 \pm 0.75 \text{ Gy ka}^{-1}$, $\log_{10}(\rho')$: -5.43 ± 0.06 and unfaded D_0 : $603 \pm 12 \text{ Gy}$. Note that the latter two parameters have been recalculated relative to the original publication using the `analyse_FadingMeasurement()` (Kreutzer and Burow, 2017) and `calc_Huntley2006()` functions respectively.

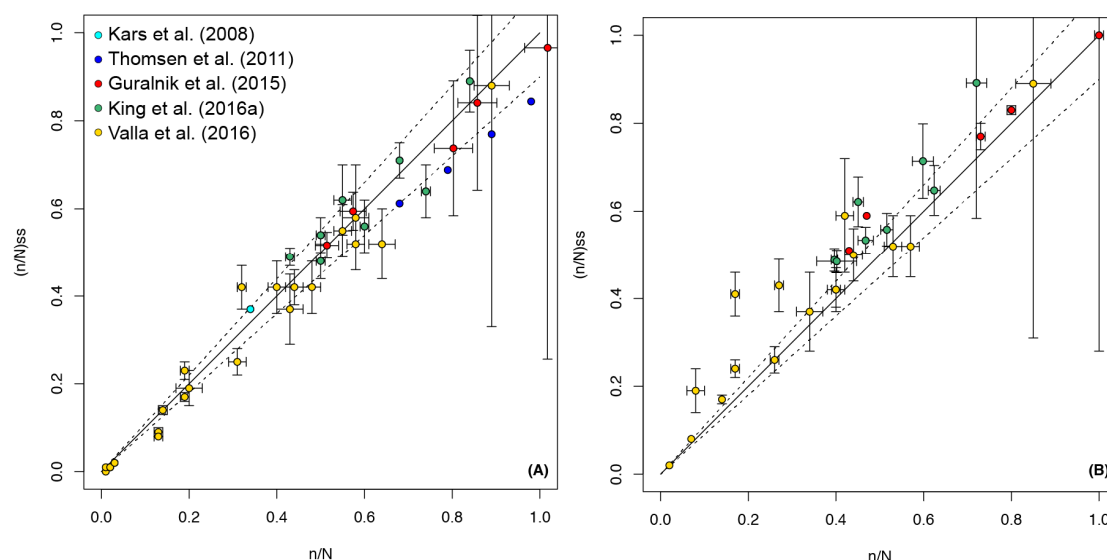


Figure 4: Comparison of (n/N) and $(n/N)_{ss}$ for published saturated samples (data summarised in Table 1) fitted with (A) a single-saturating exponential fit (1EXP, after Kars et al., 2008) and (B) a general order kinetic fit (GOK, after Guralnik et al., 2015a). A sample in saturation should have $(n/N) = (n/N)_{ss}$ and if the model performs perfectly, will sit on the 1:1 line (solid line). The data from Kars et al. (2008) and Thomsen et al. (2011) are not included in plot (B) as the raw data were not available for fitting with a GOK fit. Some of the data from Valla et al. (2016) could not be fitted robustly with a GOK fit and are not included in plot (B) (see Table 1). It is apparent that the data are less scattered when fitted with 1EXP rather than GOK which for the data of Valla et al. (2016) may relate to incomplete characterisation of the full feldspar dose response (maximum dose for some samples ~ 2.5 kGy). Although the data are scattered, for fitting with 1EXP no systematic under or overestimation of $(n/N)_{ss}$ is recorded. The majority of the data are within 10 % of the 1:1 line (dashed lines) indicating that the model has c. 10 % uncertainty when applied with 1EXP.

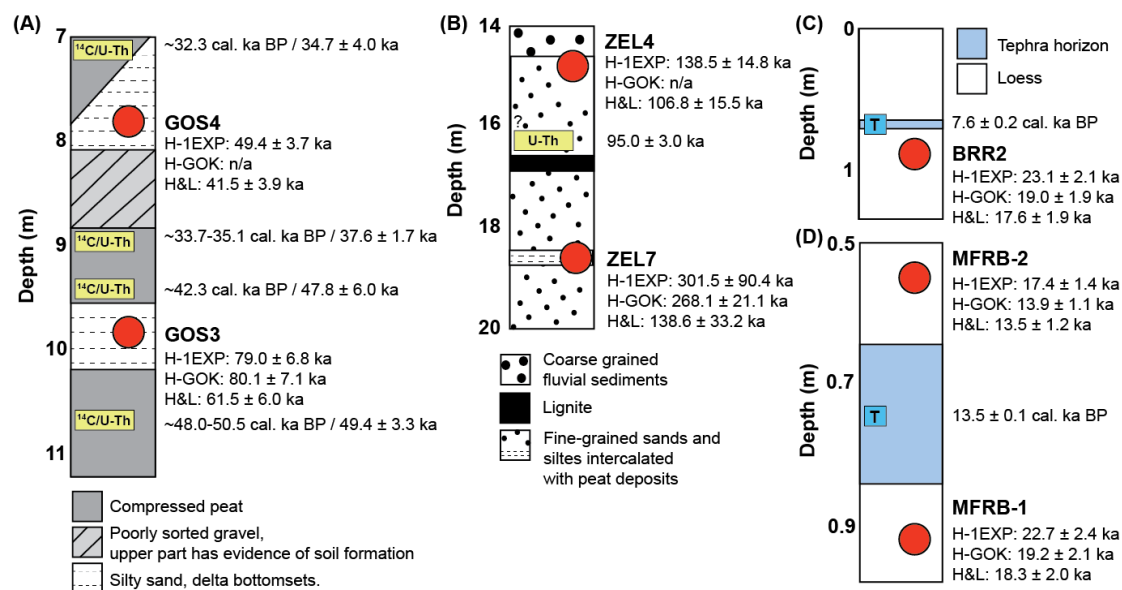


Figure 5: Approximate sample stratigraphic location and independent age control. (A) Sample locations of GOS3 and GOS4 were taken from Preusser (1999) with independent age control from Schlüchter et al. (1987) and Geyh and Schlüchter (1998). (B) Sample locations of ZEL4 and ZEL7 were taken from Preusser et al. (2001) with independent age control from Geyh et al. (1997) as described in Lowick et al. (2012). It was not possible to determine the exact location of the U/Th age at this site relative to the samples, as it is simply described as from the same unit (Lowick et al., 2012). (C) At Blackman Ridge Road (location of sample 205/BRR2) the tephra horizon is correlated to the Mazama tephra (see Figure 6); the reported age is from Adams (1990). (D) At McFeeley Road (location of samples 204/MFRB-1 and 204/MFRB-2) the tephra horizon is correlated to the Glacier Peak tephra (see Figure 6); the reported age is from Kuehn et al. (2009). H&L = Huntley and Lamothe (2001), H-1EXP = Huntley (2006) implemented with a single saturating exponential following Kars et al. (2008), H-GOK = Huntley (2006) implemented with a general order kinetic model following Guralnik et al. (2015a).

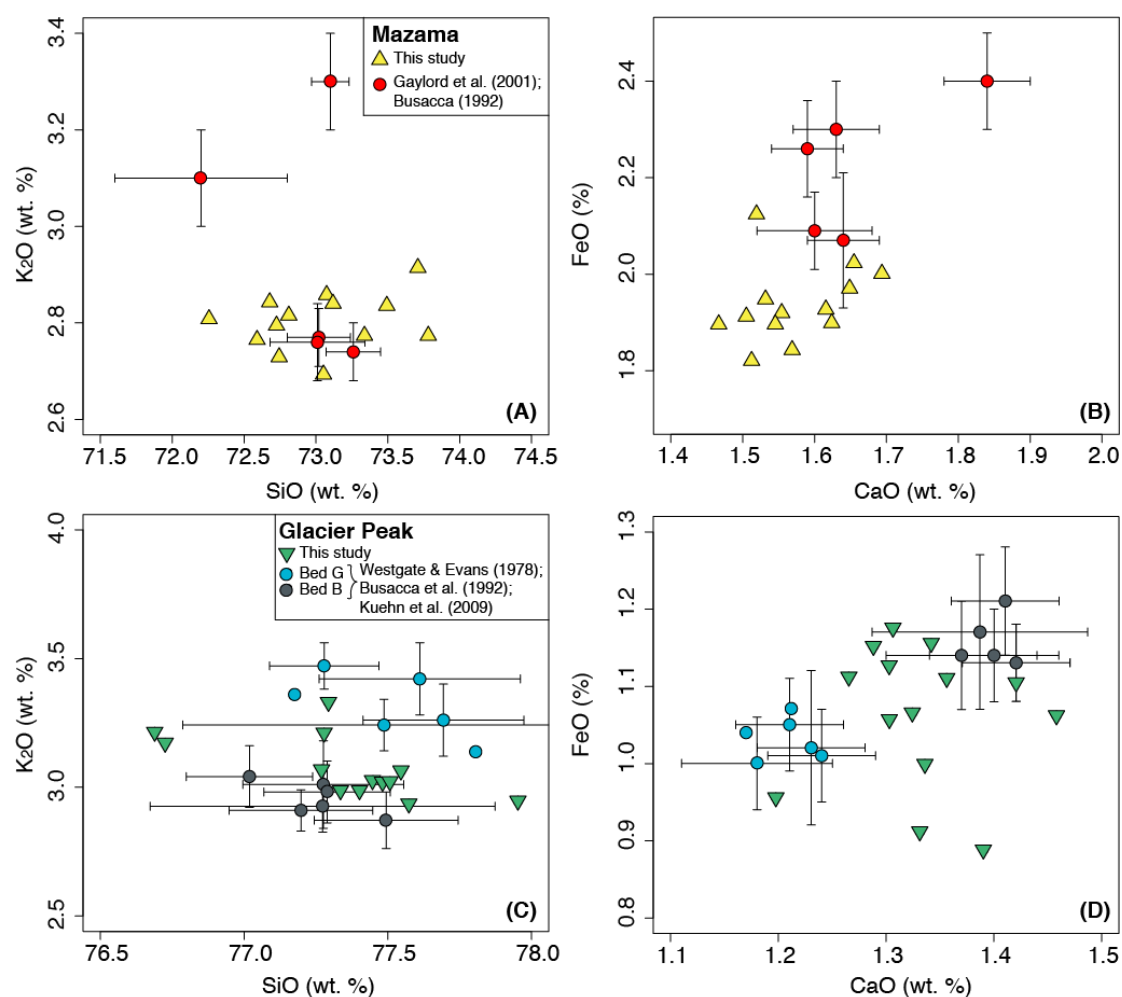


Figure 6: Comparison of tephra major element chemical data from this study, relative to previous studies (A,B) for sample BRRMAZ from Blackman Ridge Road and (C,D) for population 3 of sample MFRGP from McFeeley Road. Uncertainties are shown at 1σ for previously published data. Full chemical data are given in Supplementary Tables S.9-12.

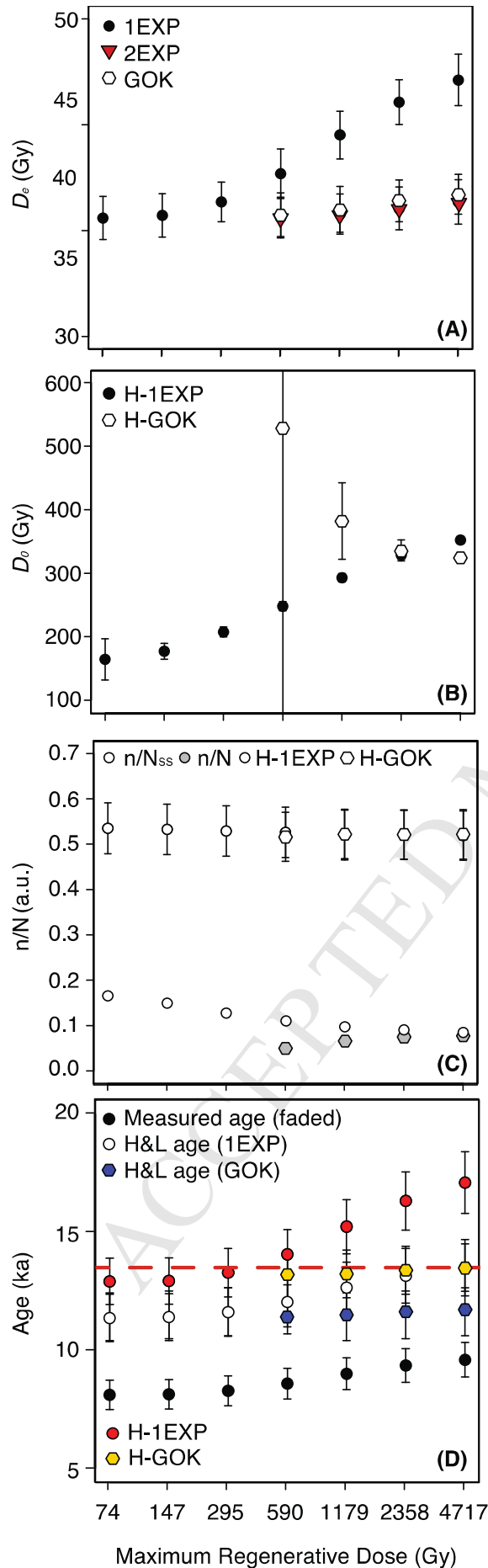


Figure 7: Effect on fitting of including additional regenerative dose points for representative sample 204/MFRB-2. (A) Changing D_e values fitted using a single or double (2EXP) saturating exponential fit, or a general order kinetic (GOK) fit using the `plot_GrowthCurve()` function (Kreutzer et al., 2012; 2018). No data are shown for the 2EXP or GOK fits for maximum regenerative doses below 590 Gy as the dose response curve is not sufficiently characterised for fitting. (B) Changing D_0 values for the 1EXP and GOK fits. (C) Changing $(n/N)_{ss}$ and (n/N) calculated using either the Huntley (2006) model after Kars et al. (2008) i.e. assuming a 1EXP fit or after Guralnik et al. (2015a,b) assuming a GOK fit. (D) Changing measured age (fitted with 1EXP), and fading corrected ages determined using the `calc_Huntley2006()` function and the Huntley and Lamothe (2001) model using the `calc_FadingCorr()` function (Kreutzer et al., 2012; 2018). The independent age control in the form of the underlying Glacier Peak tephra (Kuehn et al., 2009) is given as a red-dashed line which the luminescence ages should be younger than.

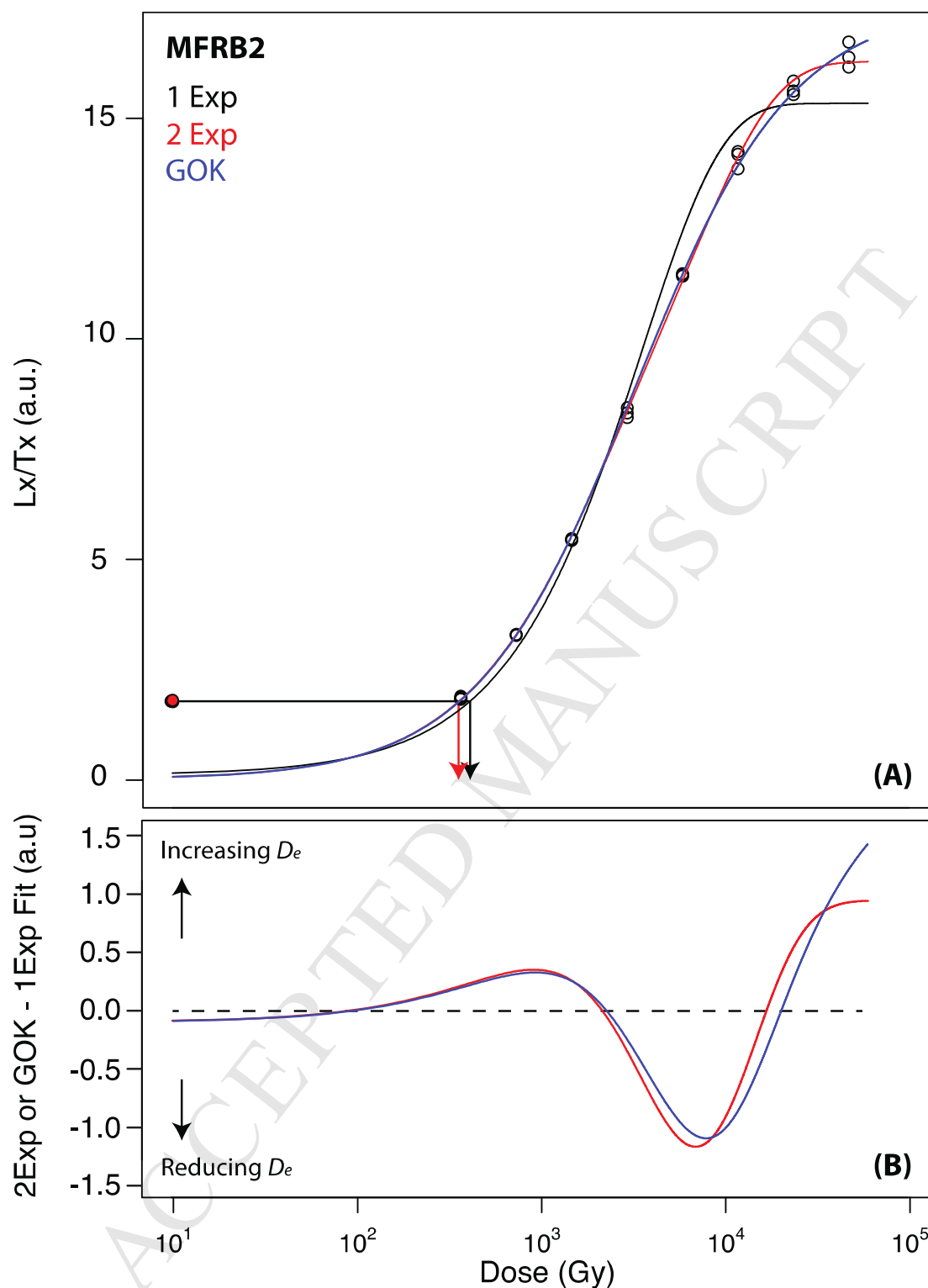


Figure 8: (A) Luminescence dose response curve of representative sample 204/MFRB-2 fitted with a single (1EXP) and double (2EXP) saturating exponential fit, and a general order kinetic (GOK) fit. Arrows show how interpolation of the same L_{nat} measurement yields different equivalent dose values depending on fit (note that interpolation of L_{nat} onto the 2EXP or GOK fit is indistinguishable). (B) Deviation of the 1EXP fit relative to the 2EXP and GOK fits.

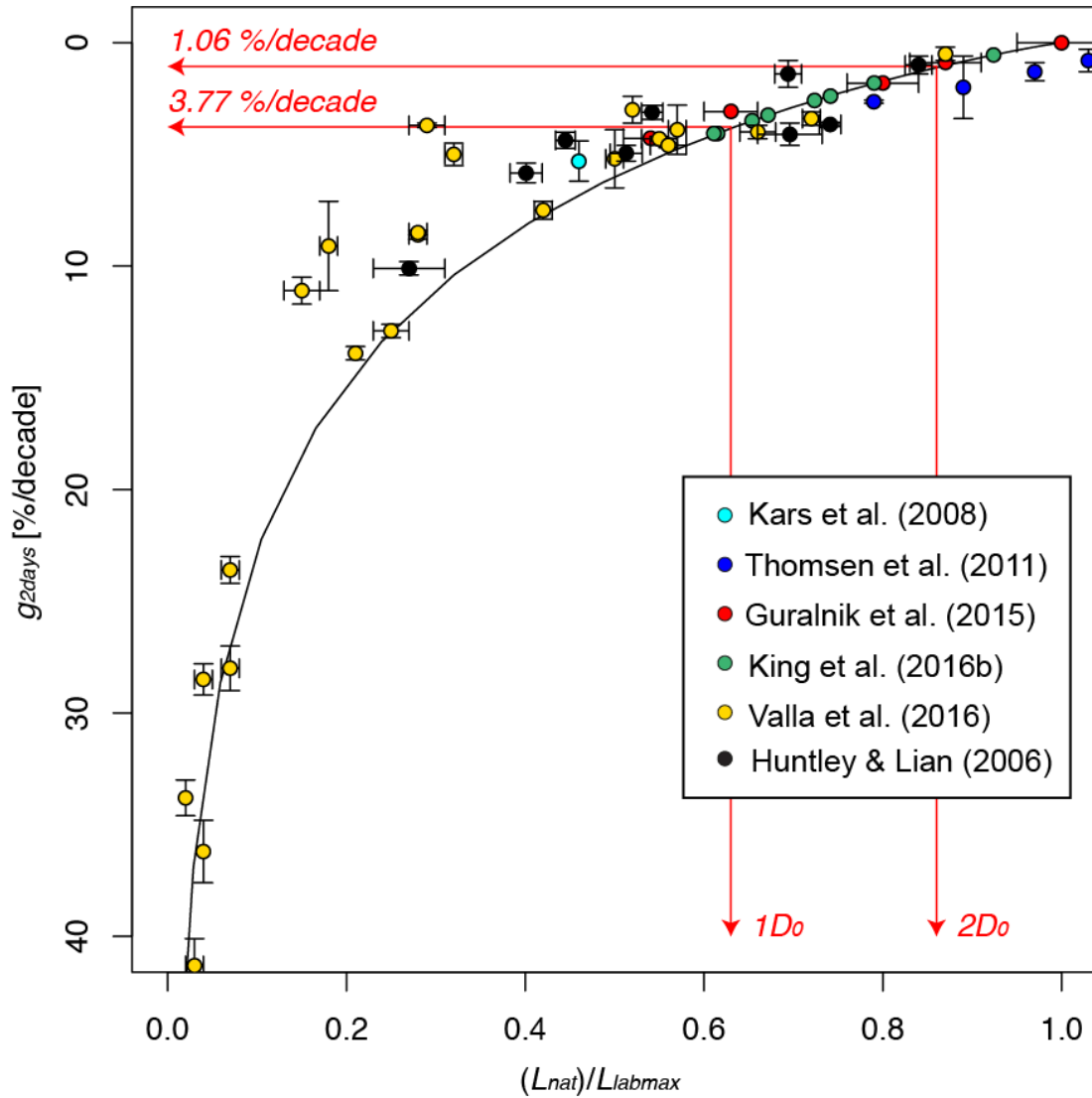


Figure 9: Modelled (line) and measured (datapoints, Table 1) $(L_{nat})/(L_{labmax})$ values for 50 samples in field saturation reported in Huntley and Lian (2006), Thomsen et al. (2011), Guralnik et al. (2015b), Valla et al. (2016) and King et al. (2016b). Modelled values are calculated assuming \dot{D} of 5 Gy ka⁻¹, D_0 of 400 Gy and a laboratory dose rate \dot{D}_{lab} of 0.134 Gy s⁻¹ using the model of Huntley (2006) implemented with a single-saturating exponential fit. The calculation is described in the main text. The red lines relate to $(L_{nat})/(L_{labmax})$ values equivalent to 1 and 2 D_0 which would be measured for saturated samples with g_{2days} of 3.77 and 1.06 %/decade respectively. Some of the scatter in the data of Valla et al. (2016) may be related to samples not being dosed completely to saturation, which could result in L_{labmax} being underestimated.

Table 1: Sample properties.

Sample Name	Description	Independent Age Control	Signal	\dot{D} (Gy ka ⁻¹)	\dot{D}_{lab} (Gy s ⁻¹)	g_{2days}^{days} (%/decade)	log10(ρ')	L_n/L_{labmax}	D_0 (Gy)	(n/N)	(n/N) _{ss}	N_{lab}/N	Pred. L_n/L_{labmax}	D_0	α	(n/N)	(n/N) _{ss}
Thomsen et al. (2008)									1EXP			GOK					
62213	Coarse grain, K-rich feldspar	Pliocene Marine Level, ~3.6 Ma	IRSL50 (Early background, post-IR protocol)	3.6	0.14	2.64 ± 0.07	1.86E-06*	0.79	425	0.68#	0.61#	0.86#	0.71#	-	-	-	-
			IRSL50 (Late background, post-IR protocol)	3.6	0.14	2.00 ± 1.40	1.38E-06*	0.89	280	0.80#	0.69#	0.89#	0.78#	-	-	-	-
			post-IR IRSL290 (Early background)	3.6	0.14	1.30 ± 0.40	8.71E-07*	0.97	610	0.90#	0.79#	0.93#	0.85#	-	-	-	-
			post-IR IRSL290 (Late background)	3.6	0.14	0.80 ± 0.50	5.13E-07*	1.03	660	0.99#	0.87#	0.96#	0.91#	-	-	-	-
Kars et al. (2008)																	
NCL-4406042 to 4406047	Coarse grain, K-rich feldspar	Late Pliocene - Early Pleistocene, ~1-3 Ma	IRSL50	2.5	0.15	5.30 ± 0.90	3.60E-06 ± 0.50E-06	0.46	529	0.34	0.37	0.74	0.50	-	-	-	-
Guralnik et al. (2015)																	
19B	Coarse grain, Na-rich feldspar	Temperature <= 33 ± 2 °C	IRSL50	1.50	0.153 to 0.180	1.68 ± 0.35	1.06E-06 ± 2.54E-07	0.80± 0.04	185 ± 12	0.80 ± 0.01	0.74 ± 0.01	0.91	0.82	170 ± 8	1.81 ± 0.56	0.73±0.01	0.77±0.03
28B				1.03	0.153 to 0.180	0.01 ± 0.12	-4.67E-09 ± 1.43E-07	1.00± 0.05	89 ± 11	1.02 ± 0.01	1.00 ± 0.74	1.00	1.00	80 ± 10	1.33 ± 1.36	1.00±0.01	1.00±0.72
105B				2.92	0.180	1.06 ± 0.21	6.93E-07 ± 1.54E-07	0.87± 0.04	193 ± 15	0.86 ± 0.01	0.83 ± 0.01	0.95	0.98	175 ± 11	1.71 ± 0.68	0.80±0.01	0.83±0.01
146A				2.84	0.153 to 0.180	3.66 ± 0.18	2.49E-06 ± 1.41E-07	0.54± 0.03	267 ± 21	0.51 ± 0.01	0.51 ± 0.00	0.80	0.58	261 ± 22	2.14 ± 0.99	0.43±0.00	0.51±0.00
218A	2.96	0.153 to 0.250	2.84 ± 0.18	1.95E-06 ± 1.66E-07	0.63± 0.03	266 ± 23	0.57 ± 0.01	0.58 ± 0.00	0.85	0.65	260 ± 59	2.25 ± 2.24	0.47±0.00	0.59±0.00			
King et al. (2016)																	
UNIL/NB19	Coarse grain, K-rich feldspar	Paired sample NBk-36-23 has an Apatite Helium age of 1.79 ± 0.06 Ma, a Zircon Helium age of 2.48 ± 0.09 Ma and an Argon-argon in Biotite age of 4.12 ± 0.1 Ma (Zeitler et al., 2014).	IRSL50 (MET)	6.62 ± 0.56	0.136	3.97 ± 0.19	2.68E-06 ± 1.43E-07	0.61%	539 ± 17	0.43 ± 0.01	0.49 ± 0.03	0.79	0.62	517 ± 18	1.75 ± 0.42	0.40±0.01	0.49±0.03
UNIL/NB19			post-IR IRSL100 (MET)	6.62 ± 0.56	0.136	2.56 ± 0.21	1.76E-06 ± 1.37E-07	0.72%	661 ± 23	0.55 ± 0.01	0.62 ± 0.05	0.86	0.72	667 ± 64	2.29 ± 0.92	0.45±0.01	0.62±0.06
UNIL/NB19			post-IR IRSL150 (MET)	6.62 ± 0.56	0.136	3.17 ± 0.17	2.16E-06 ± 1.24E-07	0.67%	667 ± 20	0.60 ± 0.02	0.56 ± 0.03	0.83	0.67	648 ± 56	2.11 ± 0.87	0.52±0.01	0.56±0.04
UNIL/NB19			post-IR IRSL225 (MET)	6.62 ± 0.56	0.136	2.39 ± 0.18	1.66E-06 ± 1.46E-07	0.74%	518 ± 19	0.74 ± 0.02	0.65 ± 0.05	0.87	0.74	475 ± 44	2.30 ± 0.96	0.62±0.01	0.65±0.06
UNIL/NB19	Coarse grain, Na-rich K-feldspar	Indicative of exhumation rates too low to be resolved by OSL-thermochronometry (c.f. King et al., 2016d)	IRSL50 (MET)	5.90 ± 0.30	0.136	3.46 ± 0.19	2.37E-06 ± 1.40E-07	0.65%	475 ± 18	0.50 ± 0.02	0.54 ± 0.03	0.82	0.65	448 ± 18	1.74 ± 0.47	0.47±0.02	0.53±0.03
UNIL/NB19			post-IR IRSL100 (MET)	5.90 ± 0.30	0.136	4.05 ± 0.21	2.68E-06 ± 1.40E-07	0.61%	618 ± 37	0.50 ± 0.06	0.48 ± 0.02	0.79	0.61	660 ± 120	2.75 ± 1.64	0.40±0.05	0.49±0.03
UNIL/NB19			post-IR IRSL150 (MET)	5.90 ± 0.30	0.136	1.92 ± 0.19	1.27E-06 ± 1.33E-07	0.79%	601 ± 19	0.69 ± 0.03	0.71 ± 0.09	0.89	0.79	576 ± 50	2.09 ± 0.90	0.60±0.02	0.71±0.08
UNIL/NB19			post-IR IRSL225 (MET)	5.90 ± 0.30	0.136	0.68 ± 0.22	4.01E-07 ± 1.59E-07	0.20%	473 ± 17	0.83 ± 0.03	0.88 ± 0.31	0.96	0.92	427 ± 36	2.15 ± 0.90	0.72±0.02	0.89±0.31
Valla et al. (2016)																	
GRA-03	Coarse grain, Na/Ca feldspar	Exhumation rates are ~0.1-0.5 km Ma ⁻¹ (e.g. Spotila et al., 2004; Berger et al., 2008)	IRSL50	1.12 ± 0.24	0.18 to 0.26	47.73 ± 0.41	2.18E-05 ± 6.75E-07	0.03 ± 0.01	622 ± 72	0.01 ± 0.00	0.00 ± 0.00	0.17	0.01	-	-	-	-
GRA-04				1.22 ± 0.23	0.18 to 0.26	28.55 ± 0.29	1.55E-05 ± 4.04E-07	0.04 ± 0.01	658 ± 90	0.02 ± 0.00	0.01 ± 0.00	0.27	0.03	-	-	-	-
GRA-05				1.31 ± 0.14	0.18 to 0.26	26.60 ± 0.80	1.44E-05 ± 1.05E-06	0.07 ± 0.01	477 ± 51	0.03 ± 0.00	0.02 ± 0.00	0.32	0.05	-	-	-	-

GRA-06			1.06 ± 0.14	0.18 to 0.26	31.23 ± 0.53	1.61E-05 ± 7.44E-07	0.04 ± 0.00	569 ± 43	0.01 ± 0.00	0.01 ± 0.00	0.29	0.04	-	-	-	-
GRA-08			1.34 ± 0.13	0.18 to 0.26	34.67 ± 1.19	1.75E-05 ± 1.31E-06	0.02 ± 0.00	562 ± 47	0.02 ± 0.00	0.01 ± 0.00	0.26	0.03	-	-	-	-
GRA-09			0.70 ± 0.15	0.18 to 0.26	24.24 ± 0.50	1.33E-05 ± 5.60E-07	0.07 ± 0.01	598 ± 54	0.03 ± 0.00	0.02 ± 0.00	0.35	0.06	708 ± 443	2.19 ± 4.13	0.02±0.00	0.02± 0.00
GRA-10			2.72 ± 0.53	0.18 to 0.26	14.92 ± 0.59	8.84E-06 ± 4.95E-07	0.25 ± 0.02	478 ± 36	0.13 ± 0.01	0.09 ± 0.00	0.51	0.19	-	-	-	-
GRA-11			1.33 ± 0.16	0.18 to 0.26	11.12 ± 0.51	6.91E-06 ± 4.32E-07	0.15 ± 0.02	410 ± 76	0.14 ± 0.01	0.14 ± 0.01	0.57	0.20	-	-	-	-
GRA-12			1.46 ± 0.22	0.18 to 0.26	15.03 ± 0.41	8.98E-06 ± 3.60E-07	0.21 ± 0.00	440 ± 22	0.13 ± 0.01	0.08 ± 0.00	0.51	0.15	547 ± 84	2.93 ± 1.30	0.09±0.01	0.07± 0.01
GRA-13			2.37 ± 0.61	0.26 to 0.27	0.47 ± 0.52	3.37E-07± 4.08E-07	0.87 ± 0.00	147 ± 9	0.90 ± 0.04	0.88 ± 0.59	0.98	0.92	434 ± 23	1.65 ± 1.88	0.85±0.02	0.90± 0.05
GRA-14			1.79 ± 0.20	0.28 to 0.29	3.49 ± 0.52	2.42E-06 ± 3.90E-07	0.72 ± 0.01	252 ± 10	0.63 ± 0.03	0.51 ± 0.08	0.83	0.61	241 ± 18	1.80 ± 0.91	0.59±0.02	0.51± 0.08
GRA-17			1.11 ± 0.35	0.12	2.95 ± 0.64	2.00E-06 ± 4.42E-07	0.52 ± 0.00	188 ± 11	0.58 ± 0.03	0.58 ± 0.13	0.85	0.66	171 ± 4	3.03 ± 0.28	0.43±0.02	0.57± 0.04
GRA-18			1.02 ± 0.39	0.12	7.59 ± 0.51	4.91E-06 ± 4.42E-07	0.42 ± 0.01	253 ± 11	0.31 ± 0.01	0.25 ± 0.03	0.68	0.38	245 ± 25	2.02 ± 1.24	0.28±0.01	0.26± 0.01
GRA-19			1.95 ± 0.39	0.12	9.02 ± 1.63	5.35E-06 ± 1.57E-06	0.18 ± 0.01	624 ± 62	0.19 ± 0.03	0.19 ± 0.05	0.60	0.25	934 ± 498	4.55 ± 4.83	0.10±0.01	0.15± 0.07
GRA-BR			3.62 ± 0.49	0.12	4.99 ± 0.62	3.22E-06 ± 4.68E-07	0.32 ± 0.01	326 ± 14	0.40 ± 0.02	0.41 ± 0.05	0.76	0.49	513 ± 192	5.81 ± 3.95	0.23±0.04	0.38± 0.03
Valla et al. (2016)																
SOG-02			8.45 ± 3.44	0.12	8.64 ± 0.46	5.38E-06 ± 4.09E-07	0.28 ± 0.01	647 ± 71	0.19 ± 0.01	0.23 ± 0.02	0.62	0.37	707 ± 419	1.85 ± 5.48	0.17±0.01	0.23± 0.02
SOG-06			9.01 ± 3.01	0.12	4.97 ± 0.41	3.23E-06 ± 3.02E-07	0.55 ± 0.02	602 ± 76	0.44 ± 0.01	0.42 ± 0.04	0.76	0.58	615 ± 282	1.58 ± 5.39	0.41±0.04	0.44± 0.09
SOG-10	Coarse grain, K-feldspar	Exhumation rates are ~0.01-0.05 km Ma ⁻¹ (e.g. Hendriks et al., 2007; Nielsen et al., 2009)	8.68 ± 3.24	0.12	4.90 ± 0.45	3.28E-06 ± 3.66E-07	0.56 ± 0.02	564 ± 64	0.48 ± 0.02	0.42 ± 0.05	0.77	0.58	590 ± 343	1.78 ± 5.96	0.40±0.05	0.44± 0.01
SOG-17			7.51 ± 3.94	0.12	4.90 ± 0.26	3.27E-06 ± 2.19E-07	0.29 ± 0.02	389 ± 82	0.33 ± 0.01	0.43 ± 0.06	0.79	0.57	383 ± 270	1.88 ± 5.01	0.29±0.02	0.45± 0.01
SOG-21			8.87 ± 3.10	0.12	10.88 ± 0.29	6.80E-06 ± 2.77E-07	0.28 ± 0.01	618 ± 95	0.19 ± 0.01	0.17 ± 0.01	0.59	0.31	728 ± 831	2.33 ± 9.10	0.16± 0.01	0.18± 0.01
SOG-22	Coarse grain, Na/Ca feldspar		1.00 ± 0.40	0.12	3.48 ± 0.31	2.35E-06 ± 2.35E-07	0.66 ± 0.02	253 ± 89	0.55 ± 0.02	0.52 ± 0.05	0.82	0.58	226 ± 161	1.40 ± 9.85	0.52± 0.02	0.48± 0.05
SOG-25	Coarse grain, K-feldspar		8.65 ± 3.19	0.12	5.63 ± 1.16	3.78E-06 ± 8.10E-07	0.50 ± 0.01	518 ± 126	0.43 ± 0.04	0.37 ± 0.09	0.75	0.54	583 ± 812	2.38 ± 11.99	0.36± 0.02	0.41± 0.06
SOG-38			8.40 ± 3.34	0.12	3.72 ± 0.31	2.50E-06 ± 2.45E-07	0.57 ± 0.01	512 ± 87	0.58 ± 0.02	0.52 ± 0.06	0.79	0.57	564 ± 806	2.40 ± 12.39	0.44± 0.02	0.45± 0.05
Huntley and Lian (2006)																
BSG1		Baltic Sea granite, Åland, Finland	-	-	1.40 ± 0.60	-	0.69 ± 0.02	-	-	-	-	-	-	-	-	-
CGS		Coryell granite, Westbridge, BC	-	-	5.83 ± 0.44	-	0.40 ± 0.02	-	-	-	-	-	-	-	-	-
MCG		Granodiorite, McKay Cr., North Vancouver, BC	-	-	1.00 ± 0.40	-	0.84 ± 0.02	-	-	-	-	-	-	-	-	-
RMG		"red granite", Rannoch Moor, UK	-	-	4.95 ± 0.35	-	0.51 ± 0.02	-	-	-	-	-	-	-	-	-
WCRS		Sanidine crystal, Kettle River Valley, BC	-	-	10.1 ± 0.30	-	0.27 ± 0.04	-	-	-	-	-	-	-	-	-
CBSS	Coarse grain, K-feldspar	Eocene or Oligocene sandstones, China Beach, Vancouver Island, Bc (Yoreth and Nasmith, 1995, p.129)	-	-	3.12 ± 0.31	-	0.54 ± 0.01	-	-	-	-	-	-	-	-	-
GP10		Pliocene Yorktown Formation, Gomez Pit, Virginia, USA (Lamothe and Auclair, 1999)	-	-	4.37 ± 0.36	-	0.45 ± 0.01	-	-	-	-	-	-	-	-	-
DY23		Red sand, Diring Yuriakh, Siberia, Russia (Mochanov, 1988)	-	-	4.10 ± 0.50	-	0.70 ± 0.04	-	-	-	-	-	-	-	-	-
TML1		Pliocene Unit, Bluefish basin, Yukon (Lamothe and Auclair, 1999)	-	-	3.66 ± 0.09	-	0.74 ± 0.01	-	-	-	-	-	-	-	-	-

Table 2 : Environmental dose rate, laboratory dose rate and fading rates for samples used in this study. Full details of the dose rate calculation for the Palouse samples (i.e. 204/MFRB-1, 204/MFRB-2 and 205/BRR-2) are given in Supplementary Material Tables S.13 and S.14. Data fitting to determine g_{2days} and ρ' for samples 204/MFRB-1, 204/MFRB-2 and 205/BRR-2 is shown in Supplementary Material S.2-4.

Sample	Environmental Dose Rate (Gy/ka)	Laboratory Dose Rate (Gy/s)	g_{2days} (%/decade)	$\log_{10}(\rho')$	Reference
204/MFRB1	4.94 ± 0.17	0.081/0.074	3.17 ± 0.28	-5.69 ± 0.05	This study.
204/MFRB2	4.39 ± 0.20	0.081/0.074	3.84 ± 0.37	-5.62 ± 0.04	This study.
205/BRR2	4.47 ± 0.22	0.081/0.074	5.62 ± 0.41	-5.45 ± 0.04	This study.
GOS3	2.70 ± 0.20	0.105	$2.65 \pm 0.42^{\$}$	-5.74^*	Preusser (1999; 2003); Lowick et al. (2012).
GOS4	2.51 ± 0.16	0.105	$2.65 \pm 0.42^{\$}$	-5.74^*	Preusser (1999; 2003); Lowick et al. (2012).
ZEL4	2.60 ± 0.20	0.105	$2.03 \pm 0.93^{\$}$	-5.84^*	Preusser et al. (2001), Lowick et al. (2012).
ZEL7	2.70 ± 0.20	0.105	$2.03 \pm 0.93^{\$}$	-5.84^*	Preusser et al. (2001), Lowick et al. (2012).

$^{\$}$ Taken from Figure 2 of Lowick et al. (2012). * ρ' not provided in the original publication; calculated from the relationship of g_{2days} and ρ' shown in the Supplementary Material.

10 Table 3: Measured equivalent dose values, and corresponding ages, as well as fading-corrected ages calculated using the Huntley (2006) model and
11 either a single-saturating exponential (1EXP) or general order kinetic (GOK) fit, and the Huntley and Lamothe (2001) approach.

Sample	n	1EXP					GOK					Independent Age Control
		Measured De (Gy)	Measured Age (ka)	Measured D ₀ (Gy)	Age (ka)	H & L Age (ka)	Measured De (Gy)	Measured Age (ka)	Measured D ₀ (Gy)	α	Age (ka)	
MFRB-1	3	68.42 ± 5.79	13.85 ± 1.47	359 ± 6	22.75 ± 2.45	18.34 ± 2.03	60.72 ± 5.03	12.29 ± 1.29	332 ± 5	1.84 ± 0.29	19.20 ± 2.12	Below Glacier Peak tephra, 13.5 ± 0.1 ka cal BP (Kuehn et al., 2009)
MFRB-2	3	42.12 ± 1.54	9.59 ± 0.77	353 ± 6	17.43 ± 1.36	13.46 ± 1.24	36.72 ± 1.45	8.36 ± 0.68	356 ± 5	1.95 ± 0.25	13.86 ± 1.08	Above Glacier Peak tephra.
BRR-2	3	44.70 ± 2.06	10.32 ± 0.94	328 ± 6	23.11 ± 2.12	17.57 ± 1.88	39.36 ± 1.89	9.09 ± 0.83	297.41 ± 5.81	1.84 ± 0.21	18.99 ± 1.88	Below Mazama tephra, 7.6 ± 0.2 ka cal BP (Adams, 1990)
GOS3	4	128.83 ± 4.23	47.71 ± 3.97	200 ± 9	79.01 ± 6.83	61.48 ± 5.98	129.54 ± 4.77	47.98 ± 4.07	421.37 ± 224.54	3.08 ± 2.93	80.09 ± 7.06	Above ¹⁴ C ages of ~48 ka cal BP and a U/Th age of 49.4 ± 3.3 ka (Schluchter et al., 1987; Geyh and Schluchter, 1998; Preusser et al., 2003)
GOS4	5	81.20 ± 3.28	32.35 ± 2.52	202 ± 8	49.35 ± 3.72	41.46 ± 3.85	-	-	-	-	-	Adjacent to peat deposit with ¹⁴ C age of ~32.3 ka cal BP and a ²³⁰ Th/U TIMS age of 34.7 ± 4 (Geyh and Schluchter, 1998). GOS4 is stratigraphically younger than GOS3.
ZEL4	4	228.02 ± 12.35	87.70 ± 8.42	274 ± 13	138.54 ± 14.79	106.76 ± 15.52	-	-	-	-	-	Samples taken from within a unit where a peat layer has been dated to 95.0 ± 3.0 ka using ²³⁰ Th/U SIMS (Geyh et al., 1997; Preusser et al., 2001; Lowick et al., 2012). ZEL4 is stratigraphically younger than ZEL7.
ZEL7	5	306.57 ± 44.33	113.54 ± 18.57	223 ± 7	293.90 ± 82.67	301.45 ± 90.38	314.47 ± 16.07	116.47 ± 10.71	361.95 ± 6.51	2.90 ± 39.75	268.11 ± 21.07	

- Fading correction of feldspar luminescence is explored using known age samples.
- Dose response deviation from a single saturating exponential causes age overestimation.
- A general order kinetic fit results in accurate age determination.
- $2D_0$ cannot be used to evaluate feldspar saturation, unless fading is corrected for.